Ocean Basin Evolution and Global-Scale Plate Reorganization Events Since Pangea Breakup

R. Dietmar Müller,[1] Maria Seton,[1] Sabin Zahirovic,[1] Simon E. Williams,[1] Kara J. Matthews,[1] Nicky M. Wright,[1] Grace E. Shephard,[2] Kayla T. Maloney,[1] Nicholas Barnett-Moore,[1] Maral Hosseinpour,[1] Dan J. Bower,[3] and John Cannon[1]

[1]EarthByte, School of Geosciences, The University of Sydney, Sydney, NSW 2006, Australia; email: dietmar.muller@sydney.edu.au

[2]Centre for Earth Evolution and Dynamics, Department of Geosciences, University of Oslo, Oslo 0316, Norway

[3]Seismological Laboratory, California Institute of Technology, Pasadena, California 91125

Annu. Rev. Earth Planet. Sci. 2016. 44:107–38

First published online as a Review in Advance on April 29, 2016

The *Annual Review of Earth and Planetary Sciences* is online at earth.annualreviews.org

This article's doi: 10.1146/annurev-earth-060115-012211

Keywords

plate tectonics, geodynamics, big data analysis, open access, open educational resources

Abstract

We present a revised global plate motion model with continuously closing plate boundaries ranging from the Triassic at 230 Ma to the present day, assess differences among alternative absolute plate motion models, and review global tectonic events. Relatively high mean absolute plate motion rates of approximately 9–10 cm yr^{-1} between 140 and 120 Ma may be related to transient plate motion accelerations driven by the successive emplacement of a sequence of large igneous provinces during that time. An event at ~100 Ma is most clearly expressed in the Indian Ocean and may reflect the initiation of Andean-style subduction along southern continental Eurasia, whereas an acceleration at ~80 Ma of mean rates from 6 to 8 cm yr^{-1} reflects the initial northward acceleration of India and simultaneous speedups of plates in the Pacific. An event at ~50 Ma expressed in relative, and some absolute, plate motion changes around the globe and in a reduction of global mean plate speeds from about 6 to 4–5 cm yr^{-1} indicates that an increase in collisional forces (such as the India–Eurasia collision) and ridge subduction events in the Pacific (such as the Izanagi–Pacific Ridge) play a significant role in modulating plate velocities.

INTRODUCTION

Conventional models of global plate motions once took the form of reconstructed map snapshots through time, often without an accompanying digital rotation model describing the motions of the plates and without present-day digital plate polygons that clarify which features on Earth's surface moved according to which plate. Most importantly, these models lacked a sense of the time-dependence of plate boundary configurations, prompting the development of a new generation of global plate motion models that reflect the dynamic nature of the plates themselves through a set of continuously closing plate polygons (Gurnis et al. 2012). These new topological plate motion models play a key role in enabling the computation of plate velocities for the entire surface of the globe through time (Zahirovic et al. 2015), for evaluating the time-dependence of the distribution of plate sizes (Morra et al. 2013), and for linking alternative plate kinematic models to global geodynamic models (Shephard et al. 2012). Equally critical is their usefulness in the computation of plate boundary lengths through time to investigate crustal production along mid-ocean ridges (Müller et al. 2013).

The ability of the geology and geophysics community to generate the next generation of plate reconstructions has been dramatically improved by the open-source GPlates software (Boyden et al. 2011, Cannon et al. 2014) and its associated Geological Information Model (Qin et al. 2012). GPlates enables the construction of global plate hierarchies and rotation files and allows the testing of alternative plate motion models. It includes the functionality to construct continuously closing plate polygons (Gurnis et al. 2012), representing a global network of moving plate boundaries that can be closed on the fly to form a complete global network of interlocking plate polygons.

The first global plate model with continuously closing plate boundaries was published by Gurnis et al. (2012) and covered most of the Cretaceous and Cenozoic periods (140 Ma to the present). It formed the basis for several studies, including a comparison of five alternative global absolute plate motion models in terms of their predicted subduction and mantle convection history (Shephard et al. 2012), an analysis of global net rotation of the plates through time (Torsvik et al. 2010), and modeling of lower mantle structure (Bower et al. 2013). This was superseded by the global plate model of Seton et al. (2012), which covers the entire time period from the breakup of Pangea to the present and contains a range of regional improvements over the previous models. Recently, this model was used to generate a detailed analysis of global plate velocities and plate events since 200 Ma (Zahirovic et al. 2015). Another distinguishing aspect of this new generation of plate models is that they include complete reconstructions of the age-area distribution of the ocean floor (Müller et al. 2013, Seton et al. 2012). This in turn facilitates an exploration of the connection between tectonic events and fluctuations in ocean chemistry (Müller et al. 2013) as well as global climate events (Huber & Goldner 2012) through time.

METHODS

The development of our global plate model involves four main components: the reconstruction of relative plate motions, an absolute reference frame, the choice of a timescale, and the construction of continuously closing plate polygons. The relative plate motion model includes a series of associated feature data, which either can help constrain relative plate motions or are derived based on the model itself. These include seafloor spreading isochrons, active and extinct mid-ocean ridge locations, the boundary between continental and oceanic crust, and an interlocking mosaic of polygons separating tectonic entities at present day (see below for details) (**Figure 1**).

Once constructed, our global plate model allows for the computation of some fundamental datasets (such as grids of the age of the oceanic crust and measures of both relative and absolute

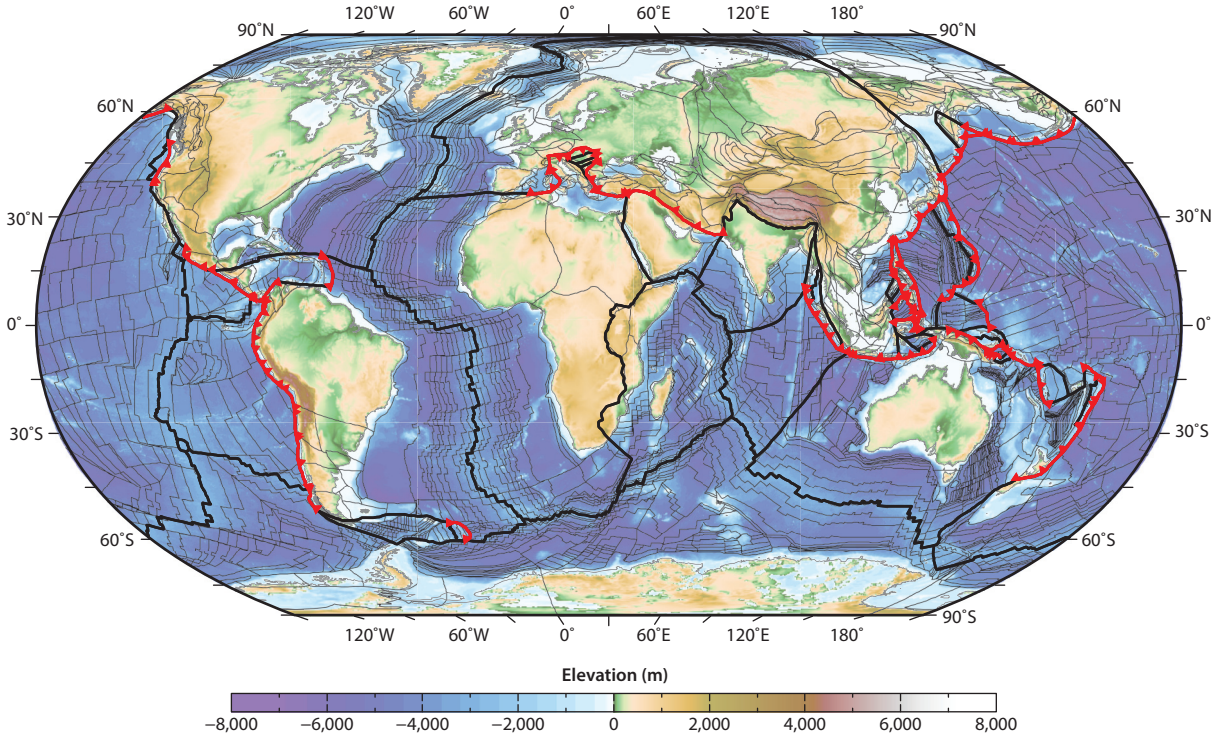

Figure 1

Global elevation model (ETOPO1; Amante & Eakins 2009), with thick black and red lines marking the outlines of present-day plate boundaries in our static polygon dataset. Seafloor spreading isochrons, shown as thin black lines, are defined as the boundaries in the oceanic realm. Present-day subduction zones according to our model are marked in red, and thick black lines mark other plate boundaries. Hammer projection with 30°E central meridian.

plate velocity magnitudes and directions) that can help elucidate global changes in the plate system through time.

Relative Plate Motions

The first two ingredients of a global relative plate motion model are a hierarchy of relative plate motion parameters (typically finite Euler rotations) embedded in an inverted tree-like structure that expresses the relationships between the plates. The relative plate motion parameters are derived from magnetic anomaly identifications (e.g., Seton et al. 2014) that are rotated along great circle arcs (following fracture zones) to compute a pole and magnitude of rotation (e.g., Hellinger 1981, Kirkwood et al. 1999). Africa is commonly used as the anchor plate at the top of the plate hierarchy due to its central position within Pangea (see Torsvik et al. 2008). The rotation tree underneath Africa expresses a cascading set of relationships describing the relative motion between the plates, which when combined with an absolute reference frame can model both relative and absolute plate motions through time.

The organization of the rotation tree is not unique, and choices are made for how to build connections between plate pairs, largely based on the presence of a continental rift or seafloor spreading margin where relative motions can be derived. In the absence of continental rifting

or seafloor spreading histories, plates are typically paired to a neighboring large plate. An example is the Philippine Sea Plate, which is almost isolated from the plate circuit by a network of subduction zones (Bird 2003), and so its motion is defined relative to the neighboring Eurasian or Pacific plates (e.g., Seton et al. 2012, Zahirovic et al. 2014). Relative motions between plates that are determined by marine magnetic anomalies and fracture zones on preserved ocean crust are considered the best-constrained parts of the plate circuit hierarchy. However, the construction of a global plate model requires reconstructing many complex, deforming regions—such as the Caribbean or Southeast Asia—where a variety of geological and geophysical constraints need to be combined. These may include structural, petrological, paleontological, stratigraphic, and age constraints from regional geology; geophysical data constraints, such as magnetic and gravity anomalies, and seismic data; and constraints on the past location of subduction zones through images of mantle seismic tomography. Paleomagnetic data may offer useful additional paleolatitudinal and block rotation constraints, but their variably large uncertainties mean that they are usually useful only when combined with other geological constraints or for times when few other constraints exist.

Seafloor Spreading Isochrons

In building our relative plate motion model, we combine published magnetic anomaly identifications (Seton et al. 2014) with the most recent interpretation of global fracture zones (Wessel et al. 2015) and derive a global set of seafloor spreading isochrons (**Figure 1**). The computation of finite rotations and construction of seafloor spreading isochrons is relatively straightforward for areas where both flanks of a spreading system are preserved, but becomes more problematic when portions of a spreading system are missing due to subduction or volcanic overprinting. When only one flank of a spreading system is preserved (e.g., Pacific–Farallon, Pacific–Kula, Pacific–Izanagi, Pacific–Phoenix), we compute half-stage rotations (stage rotation between adjacent isochrons on one flank) and double the half-stage angle (i.e., assuming that spreading was symmetrical) to create a full stage rotation. We evaluate this assumption by assessing the potential effect of spreading asymmetries on a given model (Wright et al. 2016). In instances where crust from both flanks has been subducted, we rely on the onshore geological record (e.g., mapping of major sutures, terrane boundaries, and active and ancient magmatic arcs) to help define the locations of paleo-plate boundaries and use inferences from younger, preserved crust to estimate earlier spreading directions and rates. Where continental terranes have crossed ocean basins (e.g., the Tethys Ocean), we model the history of mid-ocean ridge evolution assuming spreading symmetry, as spreading asymmetry is typically not larger than 10% for the post-Pangea seafloor spreading record (Müller et al. 1998), and ensure triple junction closure. The inferred spreading history of such a synthetic ocean basin results in a predicted subduction history, relative to the motion of the overriding plate on the side of the ocean basin where convergence occurs. Double subduction—where an ocean basin is consumed along both margins, as has recently been suggested for the Jurassic Mongol-Okhotsk Ocean (Van der Voo et al. 2015)—is rare and controversial, and it is only implemented in the plate model where the subduction histories are well documented on both active margins (e.g., Molucca Sea Plate in Southeast Asia).

The uncertainties in reconstructing mid-ocean ridges and flanks grow when moving progressively back through time as more and more mid-ocean ridge flanks that are now subducted need to be recreated in the plate model. Despite the destruction of information constraining now-subducted mid-ocean ridges, reasonable and conservative estimates as to their past geometries and locations can be made, applying Occam's razor to the application of the rules of plate tectonics (Cox & Hart 1986) in conjunction with available geophysical and geological data. It is relatively

simple to reconstruct seafloor spreading isochrons and the past age-area distribution of ocean floor in the Atlantic and Indian Oceans, where conjugate mid-ocean ridge flanks are preserved. Reconstructing the now largely destroyed Tethys Ocean basin through its various stages of opening and closing (i.e., Paleo-, Meso- and Neo-Tethys) is considerably more challenging and requires an assimilation of a diversity of geological and geophysical data. By using combined evidence from preserved magnetic lineations, geological data from accreted terranes such as "Argoland" (Gibbons et al. 2015), and the rules of plate tectonics (Cox & Hart 1986), it is possible to constrain the overall geometries of Tethys mid-ocean ridges. For the Tethys, we rely on the models by Hosseinpour et al. (2016) (western Tethys), Gibbons et al. (2015) (central Tethys), and Zahirovic et al. (2014) (eastern Tethys) for the construction of seafloor spreading isochrons and computation of gridded ocean floor ages through time.

By far the most difficult and controversial aspect of ancient ocean basin reconstructions concerns the Pacific Ocean. Preserved magnetic lineations in the Pacific Ocean provide unequivocal evidence that a vast, now largely subducted mid-ocean ridge system existed in the Pacific Ocean in the mid to Late Cretaceous, significantly longer than today's ridge system; this was first recognized by Larson & Chase (1972). Subsequent detailed mapping and compilation of magnetic M-sequence anomalies in the northwestern Pacific Ocean (Nakanishi et al. 1992) revealed the complete Mesozoic magnetic anomaly lineation pattern in this area. Nakanishi et al. (1992) observed that the reconstruction of the Late Jurassic lineations (e.g., in the East Mariana, Nauru and Central Pacific basins) reveals the exact shape of the Pacific Plate in that period, implying that the mid-ocean ridge system bounding the Pacific Plate can be reconstructed in detail all the way back to the Jurassic. Their work also revealed the origin of the Pacific Plate as a triangularly shaped microplate at a triple junction in the Panthalassa (Paleo-Pacific Ocean) basin. This work forms the basis of our Triassic–Jurassic Pacific Ocean reconstructions.

The now-vanished mid-ocean ridge that once formed part of this ridge system is the Izanagi–Pacific Ridge, which was active from about 170 to 50 Ma. Nakanishi et al. (1992) emphasized that the complete pattern of magnetic lineations preserved on the Pacific Plate reveals the configuration of the Pacific–Izanagi–Farallon triple junction, as the magnetic bight between the Japanese and Hawaiian lineation sets is clearly identified. We reconstruct the Izanagi–Farallon–Phoenix triple junction since the Late Jurassic (170 Ma) based on magnetic lineations preserved in the west Pacific Ocean (Nakanishi et al. 1992). We assume this triple junction existed in a similar form since the Triassic (i.e., 230 Ma) and rely on constant spreading rates between the Izanagi, Phoenix, and Farallon Plates from the Triassic (230 Ma) to the Late Jurassic (170 Ma). Our Jurassic–Cretaceous reconstruction of Panthalassa mostly follows those of Seton et al. (2012). Since the end of the Cretaceous Normal Polarity Superchron (CNS) at 83 Ma (also known as chron 34), our reconstructions for the Pacific Ocean are revised based on the recent work of Wright et al. (2015, 2016).

Reconstructions of Continental Rifting

The breakup of Pangea involved lengthy periods (>10 Myr) of continental rifting that ultimately led to the initiation of new seafloor spreading ridges. The quantitative reconstruction of continents during rifting relies on a diverse set of constraints, which are different from those available for periods of seafloor spreading. Estimates of syn-rift extension, together with tectonostratigraphic studies linking seismic imaging to ages of sampled syn-rift sediments and rift-associated volcanism, provide constraints on the full-fit configuration of the continents and the timing, rate, and direction of divergence during rifting. Recent advances in reconstructions take advantage of a wealth of new geophysical and geological data across rifted continental margins. Our reconstruction of Pangea breakup incorporates insights from such studies for the South Atlantic rift (Heine et al. 2013), the

Central Atlantic rift (Kneller et al. 2012), the North Atlantic–Labrador Sea rift (Barnett-Moore et al. 2016, Hosseinpour et al. 2013), and rifting between Australia and Antarctica (Williams et al. 2011).

Static Plate Polygons

A fundamental dataset that is paired with our global plate model is our present-day static plate polygons (**Figure 1**). This dataset outlines the plates and tectonic blocks that are separate tectonic entities at present day as well as plates that moved separately during some time in the past. These polygons are used to assign geodata to tectonic plates and reconstruct them according to a particular global plate motion model. This dataset differs from continuously closing plate polygon geometries (see below), which define the changing geometry of the plates via their boundaries through time.

Relative Plate Motion Noise

In recognizing regional and global tectonic events, the issue of rotation noise arises. Extremely densely sampled and interpreted marine magnetic anomaly identifications—that is, in ~1 Myr increments—require rotation smoothing, as they are subject to substantial noise that translates itself into geodynamically problematic torque acting on the plate and unreasonable fluctuations of spreading rates (Iaffaldano et al. 2014a). However, densely sampled magnetic anomaly identifications are not available for the vast majority of the ocean basins. The tectonic stages underlying our reconstructions are typically around 5 Myr long, but their length varies in time and space, reflecting which magnetic anomalies can be recognized in a given spreading regime, the picking preferences of interpreters of regional magnetic anomalies, and spatial coverage by ship tracks. Consequently, the stage boundaries underlying our global relative rotation tree vary between plate pairs.

Plate Pair Crossovers

The model includes a total of 46 plates, and the plate hierarchy expressing the relationships between these plates is composed of up to 16 hierarchical levels (at 0 Ma) (**Figure 2**). These totals reduce to 26 plates and 13 levels at 100 Ma, and then to 13 plates and 12 levels at 200 Ma. The complex changes in this plate hierarchy through time necessitate many changes in the relationships between plates—that is, the way in which fixed and moving plate pairs are arranged. We refer to a change in the fixed plate as a plate crossover. Such changes in the rotation hierarchy through time mean that crossover rotations need to be computed at the crossover time to derive an equivalent finite rotation relative to a different reference plate (**Figure 3**). For example, when a given plate B changes from moving relative to plate A to instead move relative to plate C, this shift necessitates a sequence of two finite rotations for the same age for plate B, namely, one rotation of plate B relative to fixed plate A and a second rotation of plate B relative to fixed plate C; the second rotation needs to be an equivalent rotation to the first one, using plate circuit closure. Instances where two such equivalent rotations for the same moving plate and the same age are included in the rotation hierarchy are termed plate crossovers (**Figure 3**).

Absolute Reference Frames

The anchor for any global plate motion model is an absolute reference frame that expresses how the entire system of plates moves relative to a fixed reference, such as the mantle or the spin

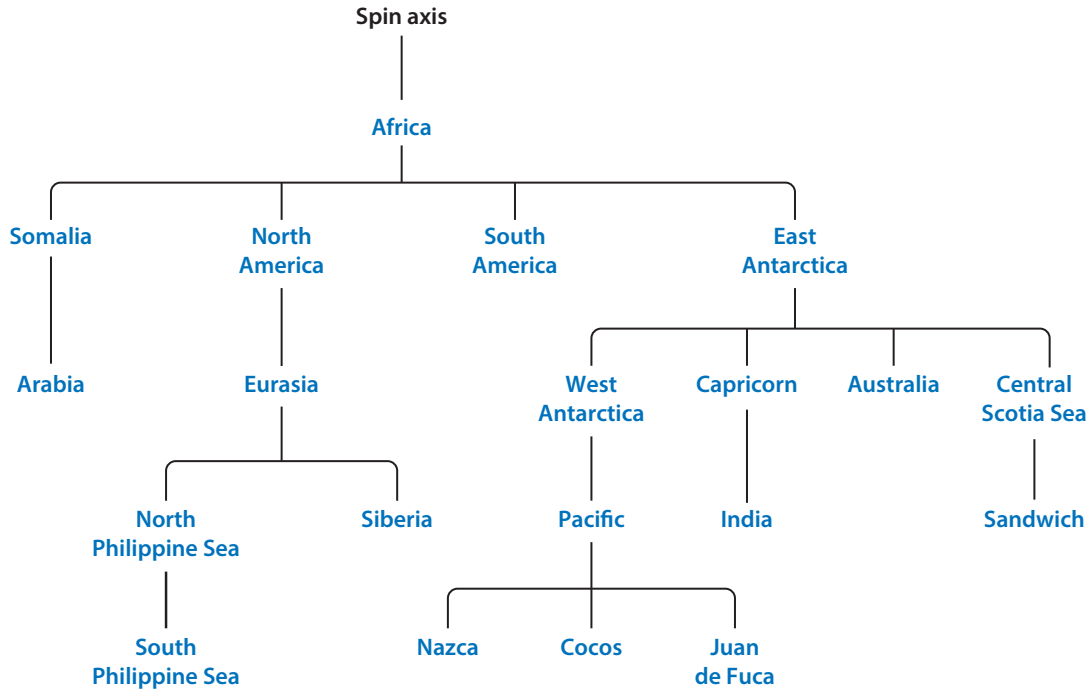

Figure 2

Illustration of part of the global plate circuit hierarchy, focusing on the connection of plates from Africa to the Pacific Ocean.

axis. Various global and Indo-Atlantic absolute plate motion models have been published relying on hotspot trails or paleomagnetic data and based on differing data, models, and assumptions. In each case these models are strictly speaking tied to the specific relative plate motion model used to link together constraints (for example, hotspot volcanism) from different plates. The hybrid absolute plate reference frame used by Seton et al. (2012) is based on a moving Indian–Atlantic hotspot model (O'Neill et al. 2005) for times younger than 100 Ma and a true polar

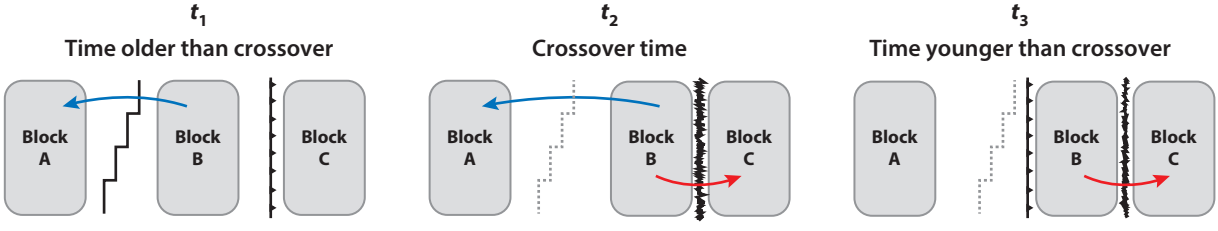

Figure 3

Illustration of plate crossovers in relative plate motions, defined as a change in the fixed plate for a given pair of moving and fixed plates. Plate motions within a global model are defined within a hierarchy of relative finite rotations. This hierarchy (i.e., plate circuit) can change through time, for instance, due to collisions after which a tectonic element (such as a continental terrane) begins moving relative to another plate. For example, at t_1 block B moves relative to block A while seafloor spreading is active. During the collision time, t_2, two equivalent finite rotations exist describing the position of block B with respect to both block A and block C at the same age. If the motion of either block A or block C, or any other plate higher in the plate hierarchy, changes during the crossover time, the equivalent finite rotations describing the crossover need to be recalculated. For a younger time t_3, the motion of block B is defined as a series of finite rotations relative to block C because a newly initiated subduction zone now interrupts the plate circuit between blocks A and B.

wander (TPW)-corrected paleomagnetic model (Steinberger & Torsvik 2008) for older times. Reassessing the optimal reference frame in the light of new data and updated relative plate motions is not straightforward, but recent studies have shown the importance of incorporating constraints from subduction zones—for example, the history of trench migration (Williams et al. 2015)—or through the seismic imaging of subducted material, which van der Meer et al. (2010) used to modify a previous hybrid reference frame. Absolute plate motion models are nearly always constructed without consideration of geodynamically reasonable trench motion behavior. Schellart et al. (2008) showed that, on average, trenches retreat slowly; specifically, trench advance or very fast trench rollback rarely exceeds 3 cm yr^{-1}. Utilizing this geodynamic rule, the quality of a number of alternative absolute plate motion models in terms of their predictions for subduction zone behavior was recently evaluated by Williams et al. (2015). Since 70 Ma, reference frames based on hotspot tracks generally provide much better constraints than other reference frames. Based on a total of five metrics related to subduction zone behavior in any given global model, the best-performing model was found to be that of Torsvik et al. (2008), which we use in our global plate model. This choice of reference frame, paired with a TPW-corrected paleomagnetic model (Steinberger & Torsvik 2008) for older times and allowing for a 35 Myr long transition period (from 70 to 105 Ma) from one reference to the other, reduces global net rotation of the plates to less than 0.4° Myr^{-1} for the entire model period and is more geodynamically reasonable than the absolute plate model used by Seton et al. (2012), which implies net rotation of the plates in excess of 0.4° Myr^{-1} at ~40–60, 65–80, 110–115, and 180–215 Ma when sampled at 1 Myr increments (Shephard et al. 2014). For times older than those well-constrained by hotspot trails (~70 Ma), longitudinal shifts of the previous hybrid reference frame have been found to better match slab remnants mapped in seismic tomography (van der Meer et al. 2010) and produce more plausible rates of trench migration between 70 and 130 Ma (Williams et al. 2015). A net longitudinal shift of 10° from 100–230 Ma is similar in magnitude to the realm of possible fits proposed by van der Meer et al. (2010), though their applied longitudinal shift of up to 18° was shown by Butterworth et al. (2014b) to be excessive, leading to substantial misalignments of modeled hotspot paths with observed hotspot tracks. This shift involves a modification to the approximated axis of TPW, whose position through time is not well known as it depends on the mantle mass distribution, reflecting subducted slabs and rising plume heads through time (Torsvik et al. 2012). We envisage that our future models of absolute plate motion will more formally incorporate geodynamic plausibility constraints.

All of the major tectonic plates, except for those within the Pacific basin, are linked to Africa via the post-Pangea seafloor spreading or rifting record back to 200 Ma (Seton et al. 2012). The Pacific Plate can be linked to the plate circuit only for times later than chron 34y (83 Ma), based on the establishment of seafloor spreading between the Pacific and West Antarctic Plates. For earlier times, the Pacific is linked to the plate circuit using a fixed Pacific hotspot reference frame (Wessel & Kroenke 2008). We assume that the Pacific reference frame is fixed relative to other hotspots, as there is no reliable model for how Pacific mantle plumes moved relative to one another or to Earth's spin axis before chron 34y (83 Ma). Similar to Seton et al. (2012), Wessel & Kroenke (2008) adjusted the Pacific hotspot rotations to avoid geodynamically unrealistic motions of the Pacific Plate by interpolating through the 118–131 Ma stage.

Timescale

All rotations and data related to our global plate model, including magnetic anomaly identifications, finite rotations, and seafloor spreading isochrons, are calibrated to one geomagnetic polarity timescale. We choose the Gee & Kent (2007) timescale, a composite in which ages younger than

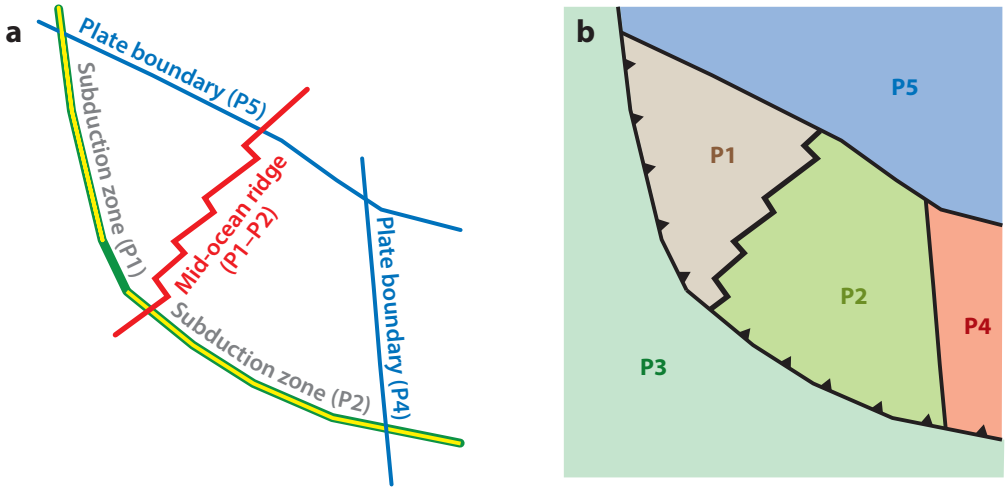

Figure 4

Schematic representation of topological plate polygon construction. (*a*) Feature geometries used to construct topological polygons. Each feature geometry is assigned information that defines the type of plate boundary (e.g., subduction zone, mid-ocean ridge) and a plate ID (P1–P5) according to which plate expresses tectonic motion relative to a fixed plate by reference to Euler rotations in the global rotation model. Mid-ocean ridge features (*red line*) are assigned left (P1) and right (P2) plate IDs based on the two plates flanking the ridge, and their motion is computed based on half-stage rotations from the relative motion between these plates. Individual geometries can be grouped into topological lines (e.g., *green line*). Both individual geometries and topological lines can be used to build topologically resolved (continuously closing plate) polygons. (*b*) Resolved plate polygons derived from geometries in panel *a*. Topological plate polygon geometries for any instant in geological time are derived from individual geometries and their intersection points using GPlates (Boyden et al. 2011).

the CNS (i.e., after chron 34y; 83 Ma) are based on the Cande & Kent (1995) timescale, with additional short subchrons summarized by Lowrie & Kent (2004), and ages older than the CNS (i.e., before M0; 120.6 Ma) are based on the Channell (1995) timescale.

Continuously Closing Plate Polygons

A network of tectonic plates, bounded by a series of independently moving plate boundaries, combines into a time-dependent topology to cover Earth's surface. Similar to Seton et al. (2012), we use the continuously closing plate methodology built into the GPlates software (Gurnis et al. 2012) (**Figure 4**) to create a new set of dynamically closed plate polygons for the past 230 Myr. The plate polygons are constructed using a series of plate boundaries, the location and timing of which have been determined by starting with present-day plate boundaries and using geological evidence for locations of island arcs, magmatic arcs, sutures, and major faults through time as well as an analysis of plate motion vectors from our kinematic model for past plate boundary geometries. We present the plate tectonic model and derive the Euler rotations (i.e., axis and magnitude of rotation) that describe the motion of each plate. Feature-specific attributes are assigned to each plate boundary feature; for example, mid-ocean ridges include information on the plate pair associated with the spreading ridge and whether it is actively spreading or extinct, which allows the mid-ocean ridge plate boundaries to be reconstructed using half-stage rotations. Subduction zones contain information regarding the polarity and duration of subduction, and transform faults track the direction of motion.

In some cases two or more topological plates share several short plate boundary sections. For example, a deforming continental margin might consist of a large number of independently moving points. Adding all these points to both the oceanic and continental plate margins that share them is time consuming and error prone. To make this process easier, GPlates supports topological lines consisting of a sequence of regular (nontopological) features that form a continuously connected dynamic polyline. This enables, for example, a single deforming line to contribute to multiple topological plate boundaries (e.g., shared by an oceanic plate and a continental plate). In this sense a topological plate boundary can be a topology of regular (nontopological) features and/or topological lines.

The continuously closed plate polygons cover the entirety of Earth's surface and are topologically valid in time intervals of 1 Myr. They can be used to compute plate velocity meshes globally or for any given tectonic plate through time, to distinguish regional from global plate events, and to capture the complex time-dependent and geometry-dependent (i.e., shape/area-dependent) velocity evolution. Even though our average tectonic stage length is about 5 Myr, the regional differences in the stage boundaries and the fact that plate topologies change continuously mean that we need to capture plate velocities at a higher resolution than that of our average stage lengths. For instance, the loss or birth of a plate may occur within a given regional stage interval due to ridge subduction, plate fragmentation, or subduction initiation, and the impact of such events on plate velocity fields will not be captured unless we compute plate velocities at 1 Myr intervals. As a consequence, we use the time-dependent topologies to extract the velocity field of plates and their continental region, for which we calculate both global and regional mean root mean square (RMS) speeds following Zahirovic et al. (2015).

RESULTS AND DISCUSSION

Global Relative Plate Motion Model

Our plate model is based on the work of Seton et al. (2012) but includes numerous regional updates and improvements (**Figure 5**). In the circum-Arctic region, we adopt the model by Shephard et al. (2013). This model includes a refined preaccretionary model for the Wrangellia Superterrane, which accretes to North America at 140 Ma, as well as a refined high-Arctic subduction history prior to the final opening of the Amerasia basin at 120 Ma. In the North Atlantic Ocean, our model incorporates new fit reconstructions from Barnett-Moore et al. (2016), in which the multiple phases of different rifting episodes in the region are accounted for, as well as updated rifting and the early postbreakup history of the Labrador Sea from Hosseinpour et al. (2013) and a refinement to the early opening history of the central North Atlantic from Hosseinpour et al. (2016).

The reconstruction for the Caribbean region has been updated following the model of Boschman et al. (2014). In the Gulf of Mexico, we implement the recently mapped extinct spreading ridge (Sandwell et al. 2014) and revised locations for the boundaries between continental and ocean crust from Christeson et al. (2014). Our revised rotations for the early central North Atlantic (Hosseinpour et al. 2016) lead to a small adjustment in the direction of seafloor spreading in the Proto-Caribbean Sea. A major plate tectonic event in the Boschman et al. (2014) model involves the capture of part of Panthalassa into the Caribbean at 135 Ma. Although Boschman et al. (2014) did not model the surrounding regions or the oceanic crust component, we find that when merged into our model for the opening of Panthalassa, the age of this trapped crust, which underlies the present-day Caribbean, is 200–180 Ma.

In the South Atlantic, our model incorporates a new early opening model based on the work of Heine et al. (2013), which argues for a relatively simple breakup history without invoking many

South American continental strike-slip faults. A recent analysis by Quirk et al. (2013) of data from the deepwater basins along the Brazilian margin provides additional support for this type of reconstruction, arguing against excessive displacements across transcontinental shear zones during South Atlantic rifting and proposing that breakup predates major salt deposits in the central South Atlantic by 6 Myr. This is important because it is a syn-rift salt deposition late-breakup scenario in the central South Atlantic that leads to a "requirement" for intracontinental shear zones. We implement the model of Eagles & Jokat (2014) for the opening of the Scotia Sea, with a minor adjustment made to the opening of the East Scotia Sea.

Recent work on the rotations of the Arabia–Africa–Somali plate pairs have been incorporated into our model, including Fournier et al.'s (2010) model for Arabia relative to Somalia & Iaffaldano et al.'s (2014b) model for Somalia relative to Africa. The Arabia–Africa rotations for closure of the Red Sea are thus indirectly derived from the rotations from these two plate pairs.

Our revised Indian Ocean reconstructions, including those of the central Tethys Ocean, are based on the work of Gibbons et al. (2015) and include southeastern Indian Ocean reconstructions from Whittaker et al. (2013). Our western Tethys and Mediterranean model represents a modified implementation of Schettino & Turco's (2011) model as described by Hosseinpour et al. (2016). To ensure plate boundary continuity between our revised model of the western Neo-Tethys and our existing model of the earlier Meso-Tethys, we adjusted the position of Iran (and therefore the Cimmerian terranes) to be aligned with the eastern Pontides, allowing for a smooth transition between Meso-Tethys closure and the subsequent evolution of the Neo-Tethys. For Southeast Asia, including Sundaland and the Proto–South China Sea, and for reconstructions of the eastern Tethys we adopt the model by Zahirovic et al. (2014).

Our Pacific Ocean reconstructions have undergone a major update, utilizing a large compilation of magnetic anomaly data (Seton et al. 2014) and fracture zone lineations (Matthews et al. 2011, Wessel et al. 2015) for the Pacific, as described by Wright et al. (2015, 2016). In addition, we have updated rotations for East–West Antarctica based on Granot et al. (2013), which significantly reduces the uncertainty in the motion of these plates. As described by Matthews et al. (2015), we extended this rotation back to 100 Ma. The southwest Pacific region, including Zealandia, was reconstructed based on Matthews et al.'s (2015) model, and the Melanesian region was modified to bridge our revised southwest Pacific and southeast Asia models to ensure plate boundary continuity between the two regions (Seton et al. 2016).

Our model for the Wrangellia Superterrane is primarily from Shephard et al. (2013) and Matthews et al. (2016a). From 230 Ma, the Cache Creek Ocean, which separates the Wrangellia Superterrane from North America, contemporaneously subducts eastward beneath western North

Figure 5

Global plate reconstructions from 230 Ma to the present day in 10 Myr intervals, showing the age-area distribution of ocean crust at the time of formation. Black toothed lines delineate subduction zones, and other black lines denote mid-ocean ridges and transform faults; beige polygons indicate products of plume-related excessive volcanism after Whittaker et al. (2015). Dark red triangles are present-day hotspot locations after Whittaker et al. (2015). Gray polygons indicate regions of nonoceanic crust, with present-day coastlines shown in dark gray. Hammer projection with 30°E central meridian. Abbreviations: A, Aluk Plate; AFR, African Plate; ANT, Antarctic Plate; AR, Arabian Plate; AUS, Australian Plate; B, Bellingshausen Plate; C, Cocos Plate; CA, Caribbean Plate; CAT, Catequil Plate; CC, Cache Creek Oceanic Plate; CHZ, Chasca Plate; CP, Capricorn Plate; EGD, East Gondwana; EUR, Eurasian Plate; FAR, Farallon Plate; GON, Gondwana; GRN, Greenland Plate; HIK, Hikurangi Plateau; IND, Indian Plate; IZA, Izanagi Plate; K, Kula Plate; LHR, Lord Howe Rise; M, Manihiki Plateau; ML, Proto-Molucca Plate; MOO, Mongol-Okhotsk Ocean; MT, Meso-Tethys Ocean; NAM, North American Plate; NAZ, Nazca Plate; NEA, northeast African Plate; NT, Neo-Tethys Ocean; NWA, northwest African Plate; PAC, Pacific Plate; PHO, Phoenix Plate; SAF, south African Plate; SAM, South American Plate; SOM, Somali Plate; SP, Sepik Plate; V, Vancouver Plate; VA, Vardar Plate; WAN, west Antarctic Plate; WGD, West Gondwana; WMT, west Meso-Tethys Ocean.

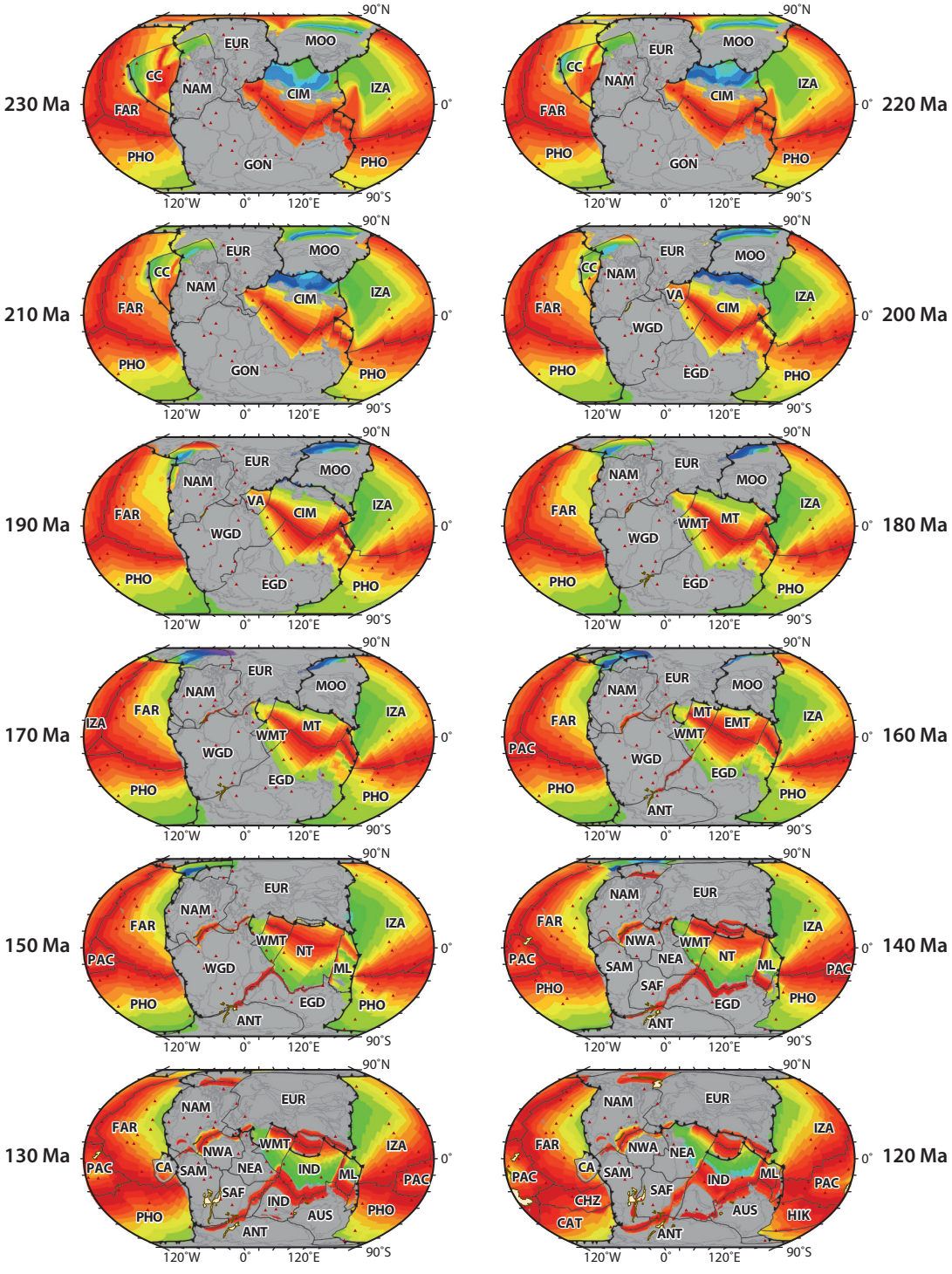
230 Ma
220 Ma
210 Ma
200 Ma
190 Ma
180 Ma
170 Ma
160 Ma
150 Ma
140 Ma
130 Ma
120 Ma
90°N
90°S
120°W
0°
120°E
EUR
MOO
CC
NAM
CIM
IZA
FAR
PHO
GON
VA
WGD
EGD
WMT
MT
EMT
PAC
ANT
NT
ML
NWA
NEA
SAM
SAF
IND
AUS
CA
CHZ
CAT
HIK
Age of oceanic crust (Myr)
0
20
40
60
80
100
120
140
160
180
200
220
240
260
280

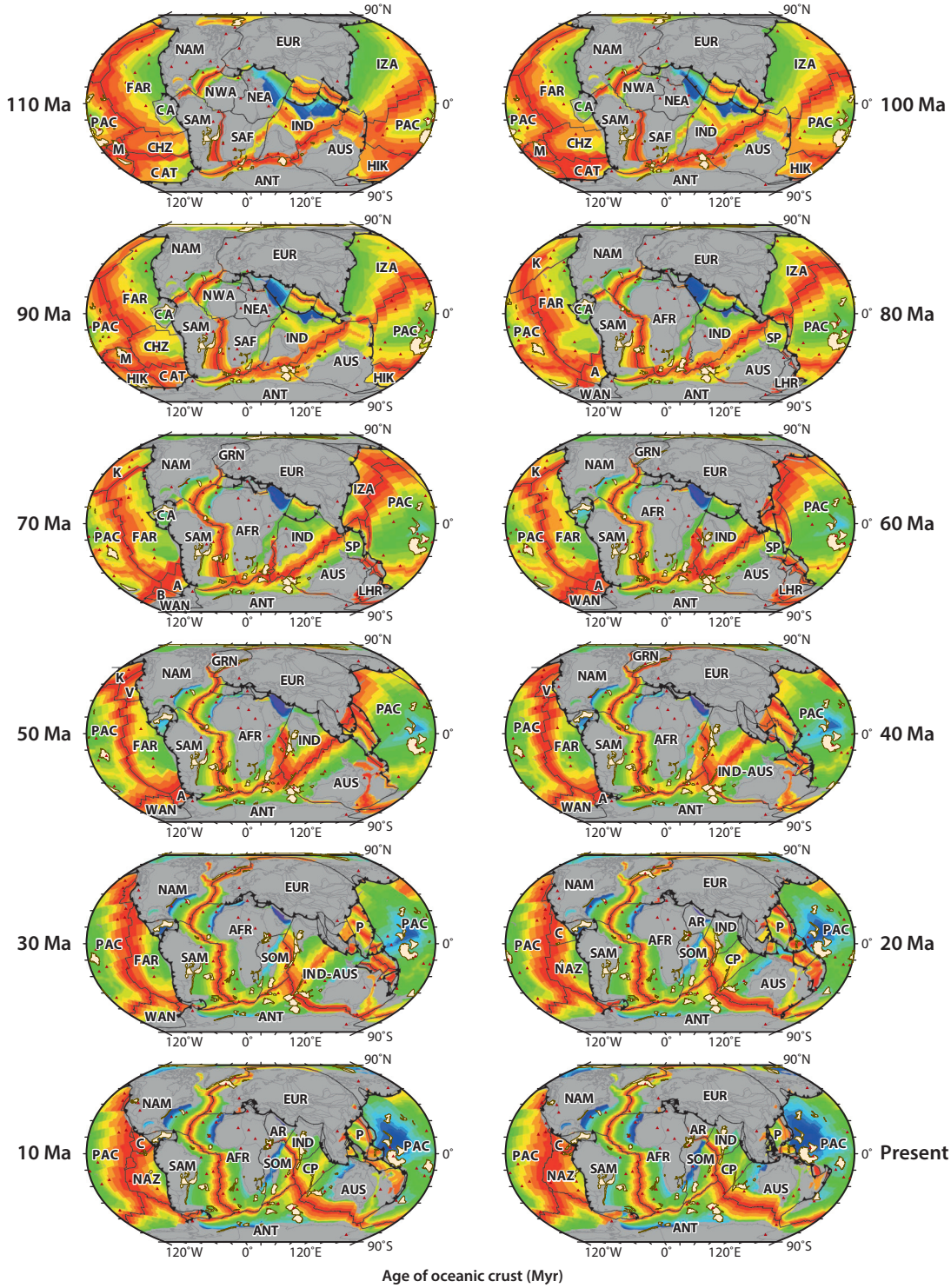
110 Ma
100 Ma
90 Ma
80 Ma
70 Ma
60 Ma
50 Ma
40 Ma
30 Ma
20 Ma
10 Ma
Present
90°N
90°S
0°
120°W
120°E
NAM
EUR
IZA
FAR
NWA
NEA
CA
PAC
SAM
AFR
IND
SAF
SP
AUS
HIK
CHZ
M
CAT
ANT
K
GRN
V
A
B
WAN
LHR
P
PAC
AR
C
SOM
CP
NAZ
IND-AUS
Age of oceanic crust (Myr)
0
20
40
60
80
100
120
140
160
180
200
220
240
260
280

America and westward beneath the superterrane (Shephard et al. 2013). A transform margin borders the Cache Creek Ocean in the north and accommodates its closure, having previously accommodated late Paleozoic back-arc basin opening behind the superterrane as it migrated into Panthalassa due to rollback of an east–northeast dipping subduction zone (Matthews et al. 2016a). A subduction polarity reversal across the Wrangellia Superterrane, from west-dipping to east-dipping subduction, occurs at 180 Ma (after Shephard et al. 2013). This coincides with docking of the superterrane with North America (Matthews et al. 2016a), which occurs 8 Myr earlier than in Seton et al.'s (2012) model. This docking is followed by a period of left-lateral transtension and subsequent transpression between 170 and 144 Ma to represent the history of the Gravina basin (Matthews et al. 2016a), which was not incorporated in Seton et al.'s (2012) model.

Oceanic Age-Area Distribution Through Time

We use our reconstructed seafloor spreading isochrons to generate oceanic paleo-age grids in 1 Myr intervals at a 0.1° grid resolution, following the method of Müller et al. (1997) (**Figure 5**). Frequency histograms of crustal age through time, binned in 10 Myr intervals (**Figure 6**), illustrate the evolution of the age-area distribution from supercontinent stability at 230 Ma through successive stages of supercontinent breakup and dispersal, with concomitant cycles of creation and destruction of mid-ocean ridge crests and flanks.

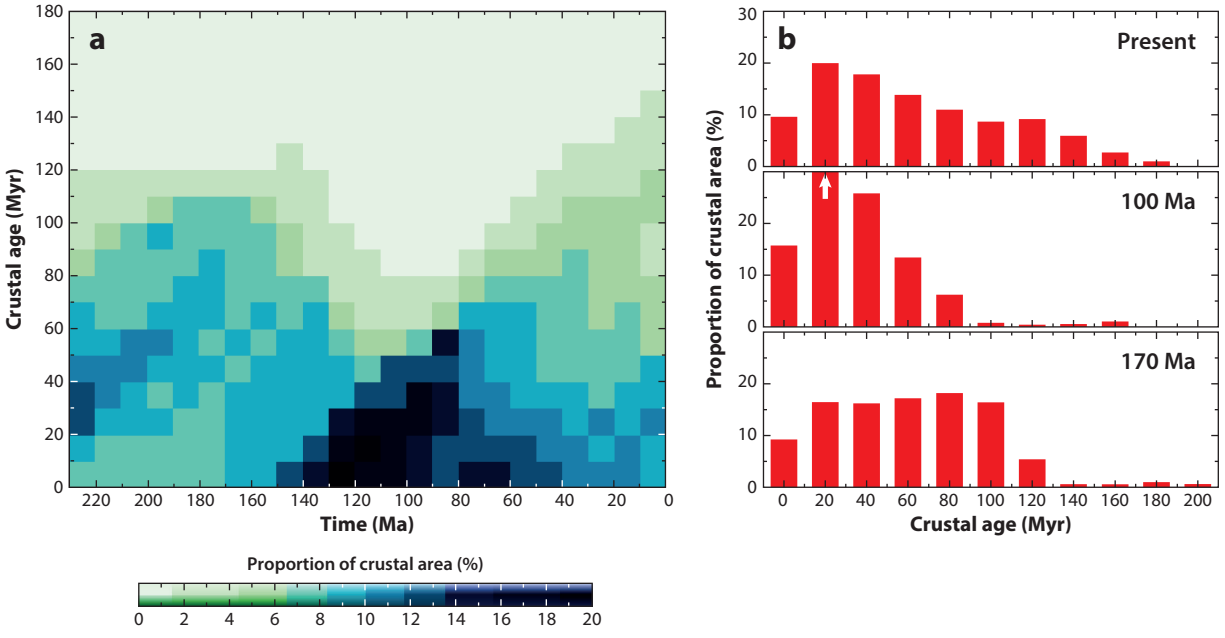

Figure 6

(*a*) Frequency histograms of crustal age through time, binned in 10 Myr intervals. The diagram illustrates significant changes through time. (*b*) The early breakup of Pangea was characterized by a roughly rectangular distribution (*bottom*), which began morphing into a progressively skewed distribution after 170 Ma due to the stepwise addition of new mid-ocean ridges and the growth of new mid-ocean ridge flanks, with a long tail of rare ocean crust older than ~90 Myr at 100 Ma (*middle*). The continued aging of mid-ocean ridge flanks and the subduction of several major mid-ocean ridges in the Cenozoic (see **Figure 5**) progressively deskew the age distribution, adding old crust and removing some younger crust, establishing the triangular distribution observed today (*top*).

The breakup of the supercontinent Pangea in the central North Atlantic around 200 Ma and the formation of the Pacific Plate around 190 Ma resulted in a 25% increase in ridge length between 200 and 150 Ma (Müller et al. 2013). These events contributed toward a substantial increase in the production rate of ocean floor and gradually changed the distribution of seafloor ages from a rectangular distribution, which is still observed at 170 Ma, to a skewed distribution in the Cretaceous; the age histogram computed for 100 Ma is a representative example (**Figure 6*b***). It shows a substantial increase in ocean floor younger than 50 Myr, reflecting the enormous growth in young ridge flank areas during the Cretaceous. After 100 Ma there was a stepwise decrease in young ocean floor due to the progressive subduction of ridge flanks, and ultimately mid-ocean ridges themselves, in the Tethys and along the Pacific Rim (**Figure 5**), paired with a continued aging of mid-ocean ridge flanks, gradually leading to the triangular distribution of seafloor ages that is observed today (**Figure 6*b***).

The uncertainties in these reconstructions cannot be formally quantified; comparisons of successive generations of models present our best opportunity to assess the effect of the underpinnings of any given model on seafloor age distributions through time, most easily captured by comparing the mean age of the ocean crust through time from alternative models (**Figure 7**). These reconstructions reflect the stepwise inclusion of an increasing amount of information though time, starting with Cogne et al. (2006), who assumed that the age-area distribution of large parts of now-subducted ocean basins never changed through time, an assumption that leads to a very significant underestimation of the changes in mean oceanic crustal age through time (**Figure 7**). Our own successive reconstructions (Müller et al. 2008, Seton et al. 2012), juxtaposed with our

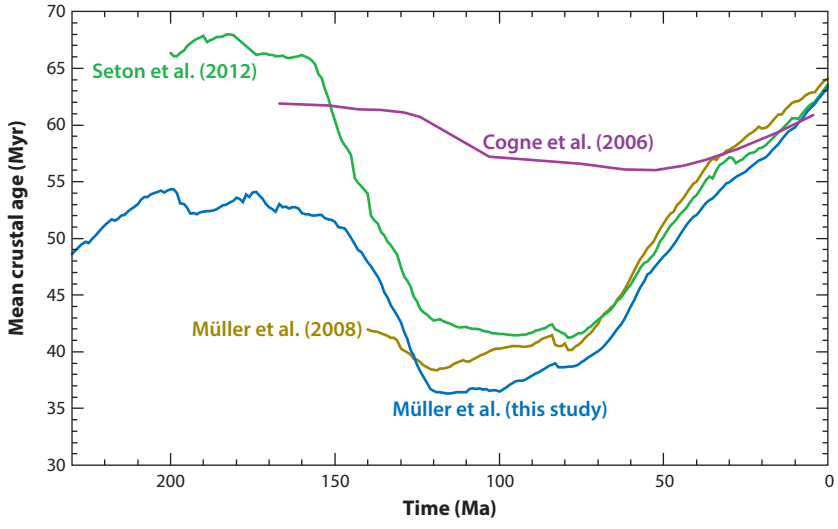

Figure 7

Mean crustal age through time in 1 Myr intervals based on our new model (*blue*) and the models by Seton et al. (2012) (*green*), Cogne et al. (2006) (*magenta*), and Müller et al. (2008) (*dark yellow*). The significant pre–150 Ma difference between the Seton et al. (2012) model and our new model is due to additional back-arc basin crust in the junction region between Panthalassa and the Tethys Ocean (see Matthews et al. 2016a) and the removal of some self-inconsistencies in the Seton et al. (2012) model in reconstructions of the Panthalassa mid-ocean ridge systems and associated rotations, especially in western Panthalassa, as discussed by Müller et al. (2014). Note the large underestimation of mean age fluctuations in the model by Cogne et al. (2006), reflecting their use of simplifying model assumptions as opposed to explicitly modeling the oceanic age-area distribution through time.

current model, reflect improvements in the modeling of complex mid-ocean ridge systems in the Pacific, reflecting the breakup of the Ontong-Java, Manihiki, and Hikurangi Plateaus (**Figure 5**) by Seton et al. (2012). Our new model also reflects the inclusion of additional back-arc basins in the eastern Tethys and around the junction between the Pacific and Tethys Oceans, following Zahirovic et al. (2014), as well as other additional changes to spreading ridges in the Indian (Gibbons et al. 2013) and Pacific (Wright et al. 2016) Oceans and the circum-Arctic (Shephard et al. 2013). The significant pre–150 Ma difference between the Seton et al. (2012) model and our new model reflects added back-arc basin crust and the removal of some self-inconsistencies in the Seton et al. (2012) model in reconstructions of the Panthalassa mid-ocean ridge systems and associated rotations, especially in western Panthalassa, as discussed by Müller et al. (2014). Both changes lead to an overall younging of the ocean basins. It should be pointed out here that our knowledge of pre-Cenozoic back-arc basins is incomplete, solely depending on information from ophiolites, which must be used to estimate the location and life span of a given back-arc basin, as well as its likely width. Successive generations of global plate models and paleo-oceanic age models will include more and more ancient back-arc basins, implying that generally we will overestimate the age of ancient ocean basins due to our incomplete knowledge of old back-arc basins.

Our model predicts major changes in seafloor age distributions through time (**Figure 6**). Such dramatic changes now have a firm geodynamic underpinning, based on the recent work of Coltice et al. (2012, 2013), who used fully dynamic mantle convection models to show that over a Wilson cycle there are variations by a factor of two in the rate of production of new seafloor, with concomitant major changes in the age-area distribution of the seafloor. In their models, supercontinent dispersal is accompanied by a skewed distribution, reflecting the progressive creation of new crust at the expense of much older crust being subducted, whereas the triangular distribution we observe today reflects a near constant production of oceanic lithosphere compared to what is destroyed (Coltice et al. 2013), as our reconstructions illustrate.

Relative Plate Motion Events

In order to analyze regional and global plate motion changes we first focus on relative plate motions, which are much better constrained than absolute plate motions. We show the rates and directions of separation between some key plate pairs along a number of representative tectonic flowlines (**Figure 8**). The images in **Figure 8** reflect full stage rotations and do not take into account spreading asymmetries. Spreading directions are computed with a fixed plate frame of choice. For a given plate pair we follow a convention in which we plot directions of relative motion for the fixed plate that is relatively higher in our plate hierarchy. The tectonic stage boundaries for each plate pair shown in **Figure 8** are subtly different, as they reflect the choices made by authors of regional plate models with respect to which magnetic anomalies are identified.

The majority of changes in rifting and spreading rates and directions shown in **Figure 8** are regional in nature. Some plate systems display major changes in rates and directions at 120 Ma, but this merely reflects the onset of the CNS close to this time, and our inability to resolve tectonic regime changes within this long period without reversals. However, recent work by Granot et al. (2012) and Granot & Dyment (2015) may open future opportunities for refining relative plate motions during the CNS. Where seafloor spreading in the CNS is partly contemporaneous with rifting along margin segments where breakup has not yet occurred, as in the South Atlantic, models based on magnetic anomalies within and bordering the CNS (Granot & Dyment 2015) need to be carefully combined with tectonic constraints from rifted margins in order to result in opening scenarios that honor tectonic constraints from rifted margins (as in Heine et al. 2013);

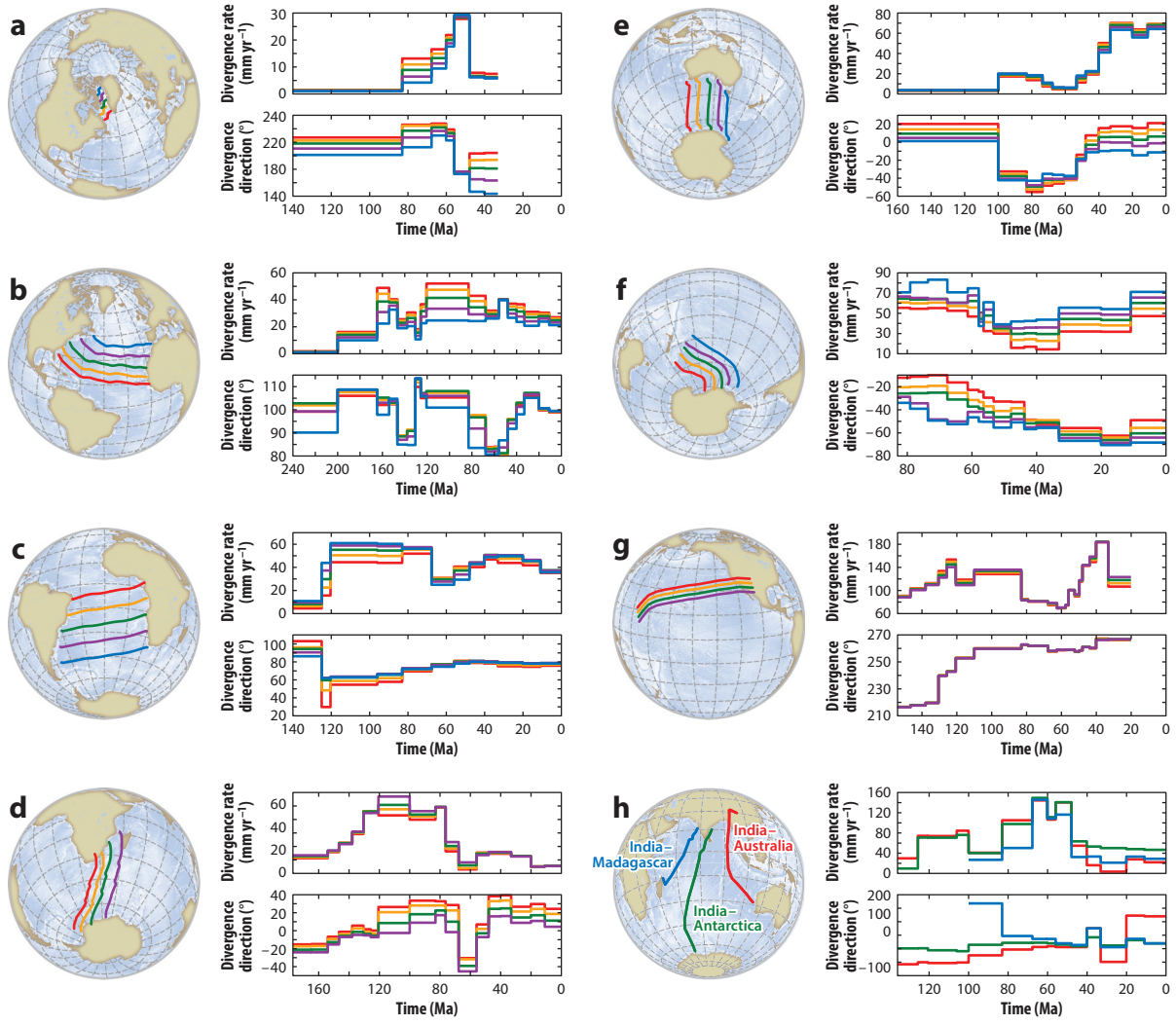

Figure 8

Rates and directions of separation between key plate pairs in our model, facilitating an analysis of regional versus global tectonic events. (*a–g*) Globes show the locations of colored tectonic flowlines (i.e., synthetic fracture zones) along which full rates of separation and directions are plotted. The colors in the rate and direction plots match those of the flowlines. (*h*) Motion paths for selected points on India relative to Madagascar, East Antarctica, and Australia. In the Indian Ocean, the complex spreading history, including major ridge jumps, means that symmetric fracture zone flowlines are not meaningful to reflect the regional relative motion history. Two events that are reflected in most plate pairs shown here occur around 80–70 and ∼50 Ma, as major changes in either spreading rates or directions. Indian Ocean divergence rates and directions are shown as synthetic plate motion paths, not following fracture zone flowlines; this is more practical for this region due to the large number of ridge jumps, which disconnect individual sets of conjugate fracture zone pairs from each other. The resulting divergence rates and directions still provide an accurate representation of relative plate motion history, revealing the ∼100 Ma change in plate motion direction between India and surrounding plates, accompanied by a slowdown in spreading, and the ∼80 Ma northward acceleration of India, expressed as an increase in full spreading rates from 40 to 100 mm yr^{-1}. Conversely, the major ∼47 Ma decrease in spreading rates records the India–Eurasia collision. The plates are as follows, with the first plate being the moving plate and second plate the fixed plate: (*a*) North America–Greenland (for Labrador Sea), (*b*) (Northwest) Africa–North America (for central North Atlantic), (*c*) (Southern) Africa–South America (for South Atlantic), (*d*) (Southern) Africa–East Antarctica (for Southwest Indian Ocean), (*e*) Australia–East Antarctica (for Southwest Indian Ocean), (*f*) Pacific–Antarctica (for South Pacific Ocean), (*g*) Pacific–Farallon (for North Pacific Ocean), and (*h*) India–Madagascar/East Antarctica/Australia.

this will be the subject of future work. A global ~100 Ma event, comprehensively discussed by Matthews et al. (2012), is more clearly expressed in the Southern Hemisphere than in the Northern Hemisphere (**Figure 8*d*,*e***); it is not visible in our South Atlantic diagram (**Figure 8*c***) as we have not yet integrated CNS magnetic anomalies (Granot & Dyment 2015) into our South Atlantic model.

Two events that are visible in nearly all the rate and direction plots in **Figure 8** occur around 80–70 and 50 Ma (in both cases ± 2 Myr). In our model of the Labrador Sea, the 70 Ma event is more subtle than the ~50 Ma event, the latter of which is expressed as a major decrease in spreading rates as well as a change in direction (**Figure 8*a***). In the central North Atlantic, the 70 Ma event is expressed as a counterclockwise change in spreading direction of ~20°, followed by a gradual clockwise change in direction starting around 50 Ma (**Figure 8*b***), whereas in the South Atlantic it is reflected by a major slowdown in spreading rates around 70 Ma, followed by a gradual acceleration in rates after ~55–50 Ma, accompanied by a gradual clockwise shift in spreading direction (**Figure 8*c***). The event is also reflected in a dramatic deceleration in spreading rates between Africa and Antarctica around 70 Ma, followed by a moderate recovery in rates after ~55 Ma, while spreading directions undergo a major counterclockwise shift around 70 Ma (between 50° and 70°, depending on location along the spreading system), followed by a stepwise clockwise shift of similar magnitude after 55 Ma (**Figure 8*d***). Contemporaneous changes in Indian Ocean tectonics have been subject to a recent detailed analysis (Cande & Patriat 2015), focusing on explanations involving plume head arrival, changes in ridge push, and collision events. Indian Ocean divergence rates illustrate the northward acceleration of India after 83 Ma, expressed as an increase in full spreading rates from 40 to 100 mm yr^{-1} (**Figure 8*b***). The exact time of the increase in India's velocity may predate 83 Ma, as this time merely marks the transition from the CNS to more frequent magnetic reversals, starting with chron 34y (83 Ma). At ~47 Ma, a major decrease in spreading rates (**Figure 8*b***) records the onset of India–Eurasia collision, consistent with a recent detailed analysis of the Indian Ocean seafloor spreading history (Cande & Patriat 2015). Onset of collision at 47 Ma is also recorded by formation of the short-lived, oceanic Mammerickx Microplate at the Indian–Antarctic spreading center, west of the Ninetyeast Ridge (Matthews et al. 2016b). Colli et al. (2014) recently analyzed the expression of the ~70–50 Ma event in the South Atlantic (**Figure 8*c***) and invoked changes in pressure-driven asthenospheric flow beneath the South Atlantic region to explain the major drop in spreading rates around 70 Ma, followed by an equivalent increase in rates, even though the ultimate driving force of such unsteady asthenospheric flow was left open.

In the Pacific, an event around 48 Ma is recorded in the Pacific–West Antarctic spreading system by a drop in spreading rate up to 15 mm yr^{-1} and a counterclockwise change in spreading direction between 1° and 8° (depending on the flowline location) (**Figure 8*f***), whereas the Pacific–Farallon/Nazca spreading center records a substantial increase in spreading rates and a small clockwise change in spreading directions between 2° and 5° (depending on flowline location) (**Figure 8*g***). To further evaluate the possible origin of these events, we next explore absolute plate motions predicted by our model as well as those based on three other published models.

Absolute Plate Motion History

Relative plate motions are intimately related to the absolute motions of plates (motion relative to Earth's deep interior). Yet, relative plate motions are much more tightly constrained than absolute plate motion models; the latter are limited by the uncertainties in geodynamic models of hotspot motion or seismic tomography imaging of the lower mantle. The detailed information contained within a relative plate motion model, together with the changing configuration of plate boundaries, provides a powerful tool to assess the likelihood of absolute plate motion change

predicted by different absolute plate motion models. For example, whether the proposed sudden change in Pacific Plate motion around Hawaiian–Emperor Bend time is consistent with relative plate motion changes or not (Wright et al. 2015), and changes in plate boundary configurations, such as subduction initiation (Arculus et al. 2015), can be assessed this way.

In order to gain some additional insights into tectonic events that have affected Africa and its adjacent continents we plot absolute RMS plate motion speeds for Africa, North America, South America, India, and Australia, paired with their plate motion azimuth through time computed at centroid points of the continents (**Figure 9**). Because all absolute plate motion models have various strengths and weaknesses depending on how they were constructed (see, e.g., Williams et al. 2015 for a recent comprehensive comparison), we compare the hybrid model we have implemented here with three other models, representing a fixed hotspot model based on African hotspots alone (Maher et al. 2015), a global moving hotspot model (Doubrovine et al. 2012), and a subduction reference model in which subducted slabs are used instead of hotspots to anchor the plates (van der Meer et al. 2010). In all three cases we use published African absolute plate rotations and link them to our revised rotation hierarchy. This may lead to inconsistencies if we were to analyze resulting plate motions for the Pacific region, as Doubrovine et al. (2012) chose a plate hierarchy different from the one used here to link the Late Cretaceous–early Cenozoic Pacific Plate to the remainder of the plate circuit. However, as we restrict ourselves to analyzing the continents around Africa, the differences between the relative plate motion models used by Doubrovine et al. (2012) and van der Meer et al. (2010) and the models used in this paper are insignificant, considering that most of the changes included in the model presented here are focused on tectonics in complex regions such as the Caribbean, the Tethys, Southeast Asia, the circum-Arctic, and the Pacific Ocean, whereas the Atlantic and Indian Ocean rotations have undergone only very minor updates. Any differences in these regions are certainly much smaller than the differences in absolute plate motions between the alternative models shown in **Figure 9**.

A model comparison for Africa is straightforward, as all absolute plate models compared here are anchored using the (South) African Plate (**Figure 9*a***). Firstly, both rates and directions of motion between our hybrid reference frame (**Figure 9*a***, gray lines) and van der Meer et al.'s (2010) reference frame (**Figure 9*a***, blue lines) are extremely similar, reflecting that the latter was built upon the former. This is also the case for all other continents analyzed (**Figure 9*b–e***). Our hybrid model results in less extreme fluctuations in rate compared with van der Meer et al.'s (2010) model, and lower Cenozoic rates of motion (around 2 cm yr^{-1} as opposed to 2–4 cm yr^{-1}). Particular care was taken for our model to ensure a smooth transition between the moving hotspot reference frame used for the past 70 Myr from Torsvik et al. (2008) and the pre–100 Ma reference frame based on paleomagnetic data. We deliberately avoid using moving hotspot reference frame rotations derived using backward advection geodynamic modeling for times before 70 Ma, as backward advection only works relatively well for about the past 70 Myr (Steinberger & O'Connell 1998). This is reflected in the original applications of this technique to modeling hotspot motion through time, which were restricted to the past 68 Myr (Steinberger & O'Connell 1998). Later extensions of this technique to longer model times, including those by O'Neill et al. (2005) and Doubrovine et al. (2012), all illustrate that backward advecting the present-day mantle structure as far back as 120 Ma is fraught with danger. As pointed out by Steinberger & O'Connell (1998), there are severe problems with "backward convection" calculations for times greater than ~70 Myr, because thermal diffusion is inherently an irreversible forward process. Once heat diffuses in a system, it is impossible to reconstruct it to its previous thermal structure. They tackled this problem by ignoring the diffusion term and advecting today's mantle density anomalies back through time, but they showed that this approach is valid only over times for which diffusion can be neglected (i.e., ~70 Myr). Some problems with Doubrovine et al.'s (2012) reference frame were highlighted by

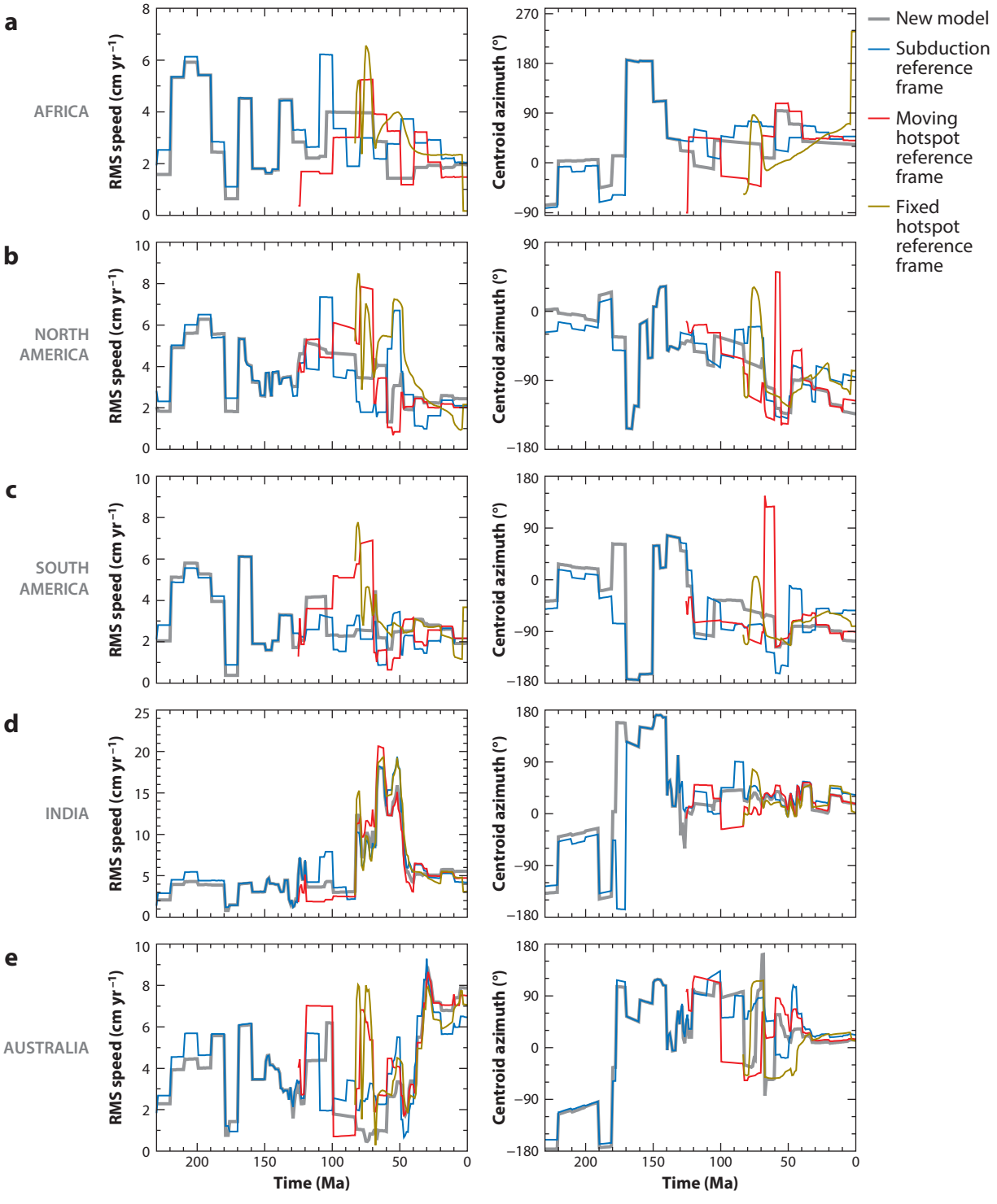
a
AFRICA
b
NORTH AMERICA
c
SOUTH AMERICA
d
INDIA
e
AUSTRALIA
RMS speed (cm yr−1)
Centroid azimuth (°)
Time (Ma)
New model
Subduction reference frame
Moving hotspot reference frame
Fixed hotspot reference frame

Williams et al. (2015), who pointed out that using this model results in a large percentage (~35%) of geodynamically unreasonably fast (>3 cm yr^{-1}) moving subduction zones, including a substantial number of advancing subduction zones for times before 70 Ma. This situation is expected to be a rarity based on the present behavior of subduction zones and geodynamic considerations (Schellart et al. 2008). Continental plate velocities based on Doubrovine et al.'s (2012) model (**Figure 9**, red lines) display much larger fluctuations than those based on the our hybrid model and Doubrovine et al.'s (2012) model for Africa and the Americas (**Figure 9*a–c***); especially noteworthy are the large fluctuations in the speed of North and South America (between 1 and 7–8 cm yr^{-1}) accompanied by back-and-forth swings in azimuth of over 60° in the period between 80 and 50 Ma.

The fixed hotspot model by Maher et al. (2015) (**Figure 9**, dark yellow lines) was constructed as an end-member test of absolute plate motions, to check how different or similar a fixed hotspot model constructed almost exclusively based on hotspots on the African Plate, bypassing plate circuit closure, would be to more complex models, which depend on a range of other assumptions (for instance, moving hotspot models depend on simplifying assumptions inherent in mantle backward advection). The model shown here is the "Chagos model" from Maher et al. (2015) that has been smoothed using the REDBACK software (Iaffaldano et al. 2014a). Even so, it still displays unreasonably large absolute plate motion fluctuations for the continents analyzed here, especially before 70 Ma (see **Figure 9*a–c***), equivalent in range to those of Doubrovine et al. (2012) (but different in timing). Neither one of these two models results in geodynamically reasonable plate motions or trench motion, following the rules of Schellart et al. (2008).

In contrast, continental plate velocities calculated using the moving hotspot model for the past 70 Myr from Torsvik et al. (2008) used in our current model (**Figure 9**, gray lines) are much better behaved in a geodynamic sense [consistent with the trench migration analysis of Williams et al. (2015)]. These results imply that despite the shortcomings of the backward advection process it is possible to design moving hotspot models at least for the past 70 Myr that result in geodynamically reasonable plate motions and trench behavior. Fixed hotspot models based on hotspots from just one plate (Maher et al. 2015) appear to be underconstrained.

Mechanisms of Plate Motion Change

We now return to major plate motion events, focusing on our current plate model. We use our global plate reconstructions and plate boundary topologies through time to derive RMS velocities for all plates through time, following the method of Zahirovic et al. (2015) (**Figure 10**), and compare them with those derived from Seton et al. (2012). Global RMS plate velocities have fluctuated between ~4 and 10 cm yr^{-1}. RMS plate speeds are reduced for many time periods, due to changes in the absolute plate model used and to the refinement of the evolution of key regions, such as the circum-Arctic (Shephard et al. 2013), the Tethys (Gibbons et al. 2015, Zahirovic et al. 2014), and the Pacific Ocean (Wright et al. 2016).

Figure 9

Continental absolute plate velocities divided into root mean square (RMS) rates (*left column*) and directions (azimuth clockwise from North) computed at a given continent's centroid point (*right column*) for (*a*) Africa, (*b*) North America, (*c*) South America, (*d*) India, and (*e*) Australia. Our new model (*gray*) is compared against continental velocities resulting from van der Meer et al.'s (2010) subduction reference frame (*blue*), Doubrovine et al.'s (2012) moving hotspot reference frame (*red*), and Maher et al.'s (2015) African fixed hotspot reference frame (*dark yellow*). In the latter three cases we have combined published absolute plate rotations for Africa with our revised relative plate motion model.

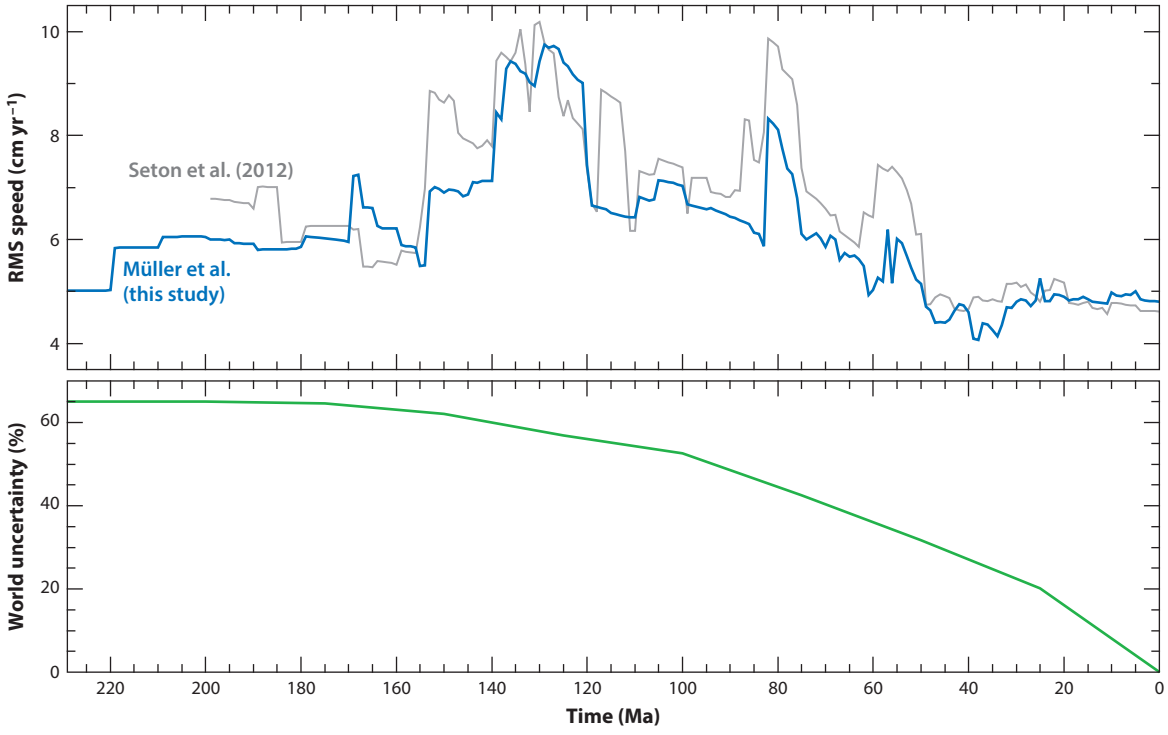

Figure 10

Global root mean square (RMS) plate speeds from our new model (*blue*) compared with those from Seton et al. (2012) (*gray*), with world uncertainty of preserved lithosphere following Torsvik et al. (2010). One of the most noticeable features is the relatively fast global plate motion in the Early Cretaceous from 140 to 120 Ma, corresponding to the most intense period of plume activity and large igneous province emplacement since the Jurassic (Prokoph et al. 2013).

High RMS rates of around 9–10 cm yr^{-1} from 140 to 120 Ma correspond to a time of massive emplacement of large igneous provinces (LIPs) (Prokoph et al. 2013). The consecutive mantle plume heads impinging on the plates during this time may have led to a change in plate-mantle coupling and a transient period of accelerated global spreading rates (Müller et al. 2013), which then also lead to an increase in global RMS velocities. These LIPs include Paraná-Etendeka (135 Ma) (Dodd et al. 2015), Gascoyne (136 Ma), Piñón (123 Ma), Manihiki (123 Ma), Ontong-Java and Hikurangi (122 Ma), and Kerguelen (118 Ma) (Prokoph et al. 2013). It is worth noting in this context that the age range of LIP emplacement is likely underestimated for all oceanic plateaus, due to very limited data coverage usually restricted to the very top of these edifices (Whittaker et al. 2015). Kumar et al. (2007) suggested that the multiple plumes would thin the lithosphere and weaken the lithosphere-asthenosphere coupling, leading to an increased effectiveness of ridge push and slab pull, even if these forces remain constant. Such a mechanism may have led to the modeled increase in RMS velocities between 140 and 120 Ma.

A major plate reorganization is recorded in continental geology and seafloor fabric during the mid-Cretaceous, with the synthesis by Matthews et al. (2012) suggesting a major global perturbation to plate motions at ~105–100 Ma. Because this plate reorganization occurs during the CNS, dating the change in plate motions requires interpolation of ages during the CNS, as well as basement ages at Deep Sea Drilling Project sites and other dating techniques on the continents

(e.g., major changes in volcanism) (Matthews et al. 2012). The reorganization manifests itself in major changes of the India–Antarctica and India–Australia seafloor spreading rates and directions (**Figure 8*b***). The change from largely northwestward motion of India to largely northward convergence with Eurasia from ∼100 Ma has been previously suggested to result from the initiation of Andean-style subduction along southern continental Eurasia, with ongoing and contemporaneous intraoceanic subduction in the Neo-Tethys (Gibbons et al. 2015). The reorganization in the Neo-Tethys is coeval with the slowdown in Australia's absolute motion close to 100 Ma from ∼6 to 2 cm yr^{-1} RMS speed (**Figure 9**), associated with cessation of long-lived East Gondwana subduction (Matthews et al. 2012), as well as major changes in the Atlantic and Pacific Ocean basins. In the central North and South Atlantic, an increase in seafloor spreading rate at ∼105–100 Ma and a change in the seafloor fabric (Matthews et al. 2012) may be linked to the changes in the absolute motions of Africa and South America (**Figure 9**). In addition, a significant reorientation of the hotspot trails at 95 ± 8 Ma in the Pacific (Wessel & Kroenke 2008) highlights the global nature and synchroneity of the major plate reorganization event (Matthews et al. 2012). A short increase in RMS speed centered on ∼80 Ma reflects an increase in speed in India's plate motion and most plates in the Pacific Ocean basin. Both the amplitude and timing of this event are uncertain, as the event corresponds to the end of the CNS, and the topologies of the now-subducted portions of plates in the Pacific, which underpin this result, are not well known.

Our plate model indicates that Africa slowed down substantially after 70 Ma (**Figure 11**), effectively halving its speed from 4 to 2 cm yr^{-1}. This occurred before Africa was involved in any major collisions along its northern boundary, and the change was not accompanied by any major changes in subduction zone geometry in the western Tethys (**Figure 5**). As pointed out by Cande & Patriat (2015), India sped up initially during this process, which can also be seen in **Figure 9*d***, but slowed down again after 47 Ma due to the stepwise collision of India with Eurasia. South America slowed down somewhat during this period; the magnitude of the slowdown depends on the absolute plate motion model (**Figure 9*c***). Our model suggests a decrease on the order of about 1 cm yr^{-1}, followed by a similar increase after 50 Ma.

In order to shed additional light on plate motion changes experienced by South America during this period, we plot the subducting crustal age along the South American trench as a function of distance as well as the mean age and standard deviation of the subducting ocean crust through time (**Figure 12**). The time period between 80 and 40 Ma is characterized by a two-stage evolution. First, the Farallon–Aluk Ridge starts being subducted along southern South America, resulting in a substantial younging of the ocean flow being subducted along this region (**Figure 12**). After about 70 Ma the age distribution of the downgoing plate develops a dichotomy, with the age of the subducting plate gradually increasing along the northern two-thirds of the trench, from about 50–60 to 80–100 million years, but this process only leads to a marked increase in the mean age of the subducting plate, by about 10 million years, after about 55–50 Ma.

Following the geodynamic modeling of Goes et al. (2008), younger lithosphere should be less able to drive trench retreat, so faster rollback should be driven by relatively older lithosphere, exerting a larger suction force on the overriding plate. Perhaps the slowdown of South America–Africa seafloor spreading after ∼70 Ma is a consequence of the major younging of ocean floor along the southern 2,500 km long segment of the Andes, whereas the progressive aging of the downgoing ocean floor along the northern two-thirds of the Andes after 55–50 Ma may have led to an increase in trench rollback speed and suction force, accelerating spreading rates. This model would present an alternative to the unsteady asthenospheric flow hypothesis suggested by Colli et al. (2014) for these spreading rate variations. However, even if the process suggested here (based on **Figure 12**) made a contribution to modulating the spreading rates in the South Atlantic, it cannot explain the slowdown of Africa after 70 Ma. This observation may be accounted for by the

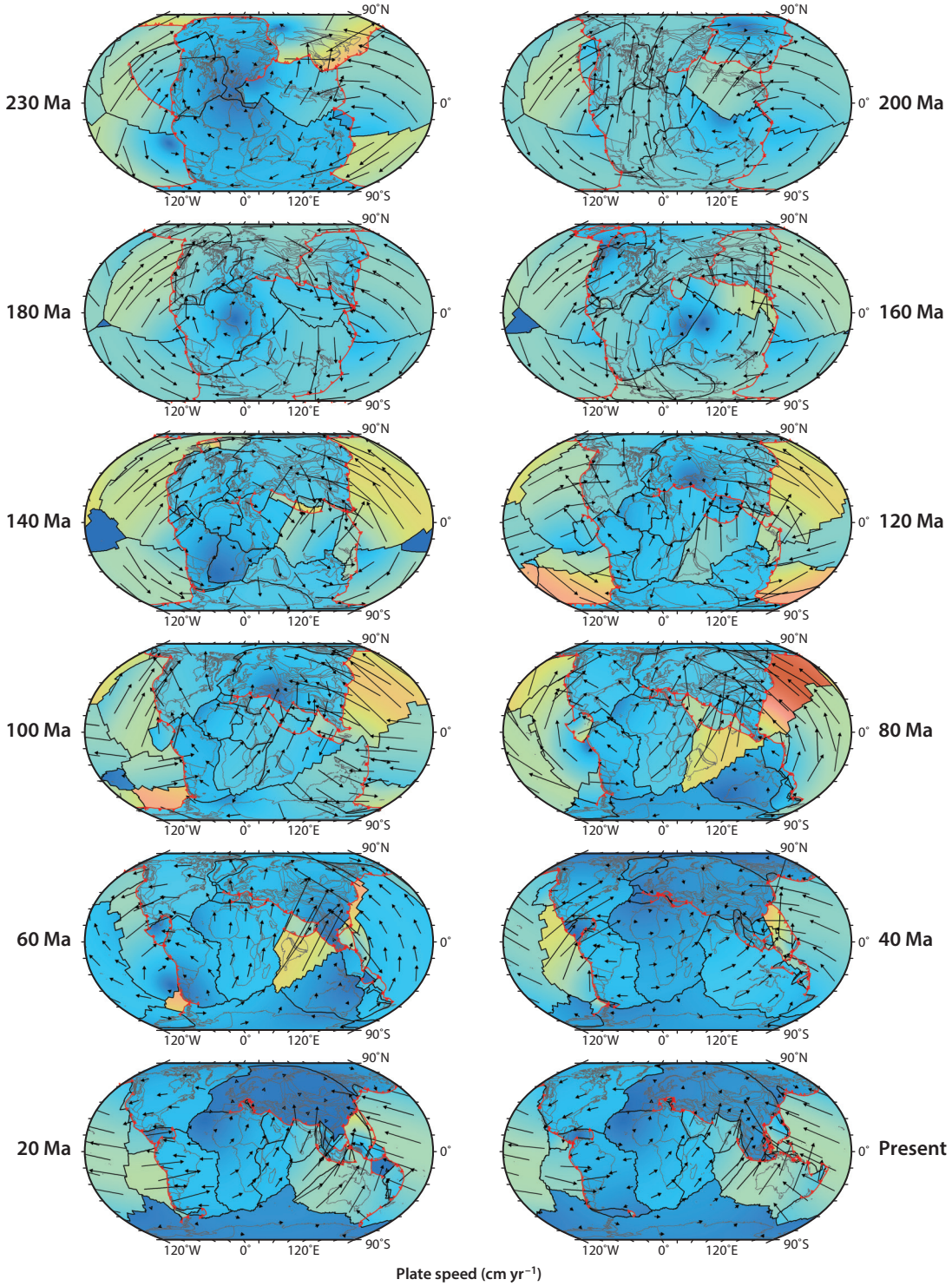
230 Ma
200 Ma
180 Ma
160 Ma
140 Ma
120 Ma
100 Ma
80 Ma
60 Ma
40 Ma
20 Ma
Present
90°N
0°
90°S
120°W
120°E
Plate speed (cm yr−1)
0
5
10
15
20

model presented by Capitanio et al. (2009), who proposed avalanching of the slab attached to the northern margin of Africa around 50 Ma, following stagnation on the preceding 20 Myr. This model explains not only Africa's slowdown around 70 Ma, but also its speedup around 50 Ma.

Beyond this regional effect, there is evidence for a global-scale ~50 Ma event that expresses itself not only in regional relative plate motion changes in most ocean basins (**Figure 8**; see also the summary in Whittaker et al. 2007), but also in a decrease in global absolute RMS plate speeds around that time. The origin of that event remains unclear, as it does not appear to be directly related to the Hawaiian–Emperor Bend, which mainly reflects the slowdown of southward motion of the Hawaii plume (Tarduno 2007, Wright et al. 2015). However, the Hawaiian–Emperor Bend may still include a component of absolute plate motion change, as the reorganization of the mantle flow processes beneath the Pacific that led to the slowdown of the Hawaiian plume may have had a feedback effect on plate-mantle coupling and absolute plate motions. In one possibility for such a process, outlined by Seton et al. (2015), complete Izanagi plate subduction and margin-wide slab detachment, followed by reinitiation of subduction along the Izu–Bonin–Mariana (IBM) arc between 52 and 48 Ma (Arculus et al. 2015), could induce a major change in sub-Pacific lower mantle flow, from dominantly southward before 60 Ma to north-northeastward after 50 Ma, ultimately leading to a global change in plate-mantle coupling.

The "50 million year event" (Whittaker et al. 2007), visible in relative and absolute motion changes in many parts of the globe (**Figures 8** and **9**), expresses itself in a reduction in global RMS velocities from about 6 to 4–5 cm yr^{-1} (**Figure 10**). If a sudden westward acceleration of the large Pacific Plate following IBM subduction initiation (Arculus et al. 2015) had been the sole or main effect of the 50 Ma event, we should see an increase in RMS speeds, rather than the decrease we observe in our model. Using forward geodynamic modeling, Butterworth et al. (2014a) showed that the Pacific Plate underwent a relatively minor speedup following IBM subduction initiation. These model results are also consistent with the very gradual speedup in spreading rates between the Pacific and Farallon Plates after IBM subduction initiation around 50 Ma, drawn out over 10 Myr (Wright et al. 2015) (see also **Figure 8*g***). All these models and observations consistently point to a plate-mantle reorganization starting around 50 Ma, likely caused by IBM subduction initiation, but with the kinematic changes in regional Pacific relative and absolute plate motions alone not sufficient to cause the Hawaiian–Emperor Bend (Butterworth et al. 2014a, Tarduno 2007, Wright et al. 2015). It is significant that IBM subduction initiation is only slightly predated by a collisional event—namely, the onset of collision between India and Eurasia, likely recorded by the major slowdown in spreading rates between India and Eurasia (**Figure 8*b***) (Cande & Patriat 2015, Capitanio et al. 2009, Gibbons et al. 2015) and oceanic microplate formation at the Indian–Antarctic spreading ridge (Matthews et al. 2016a) around 47 Ma—leading to an amplification of the ~50 Ma event globally. Rona & Richardson (1978) originally suggested that the Eocene global plate reorganization primarily reflects an increase in collisional forces resisting plate motions. The slowdown in RMS speeds around 50 Ma resulting from our global plate velocity analysis (**Figure 10**) indeed suggests an increase in forces resisting plate motions as a key factor in driving this global event. It follows that Izanagi–Pacific Ridge subduction (Whittaker et al. 2007) and IBM subduction initiation (Arculus et al. 2015) may have mainly affected circum-Pacific plate-mantle dynamics,

Figure 11

Reconstructions of absolute plate velocities, with colors and vector lengths indicating plate speed and vector azimuths representing absolute plate motion directions. Subduction zones are shown as red toothed lines that indicate subduction polarity, mid-ocean ridges are shown as black lines, and coastlines and boundaries between continental blocks and terranes are shown as gray lines. Hammer projection with 30°E central meridian.

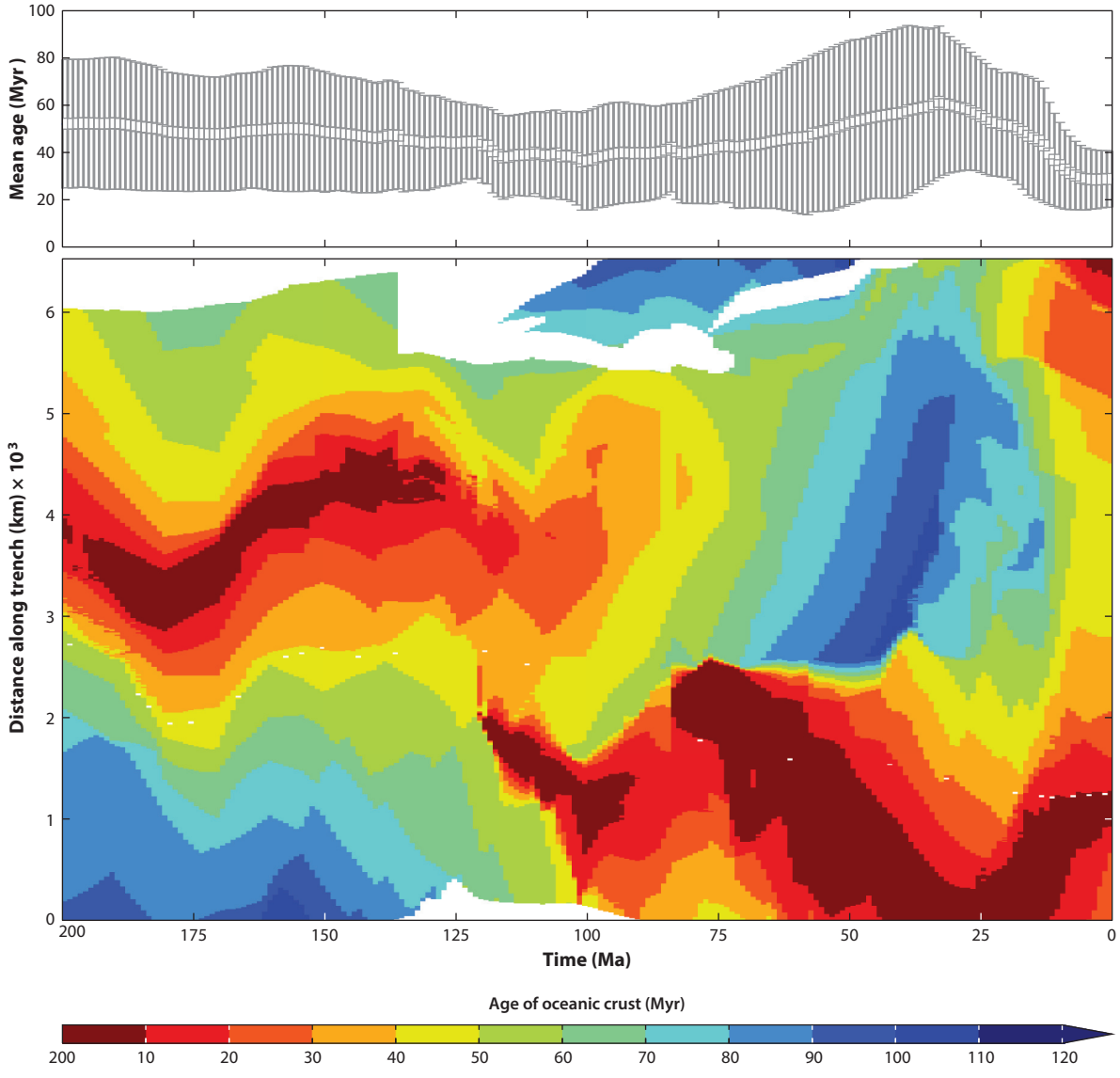

Figure 12

Mean age and standard deviation (*top*) of subducting ocean crust computed along the South American subduction zone along a 6,500 km long profile from south to north, showing subducting crustal age at the trench as a function of distance (*bottom*). The relatively young ocean crust subducted along the mid-section of the trench between 200 and 100 Ma mainly corresponds to the subducting Farallon–Phoenix mid-ocean ridge (**Figure 5**), whereas after 120 Ma, fragmentation of the Phoenix Plate led to the formation of an additional mid-ocean ridge system between the Chasca and Catequil Plates (Seton et al. 2012), intersecting the trench further south from 120 to ~90 Ma (**Figure 5**). After 90 Ma the Farallon–Aluk Ridge, and later the Nazca–Aluk Ridge, is being subducted along southern South America (**Figure 5**), resulting in a growing N–S subducting age asymmetry along the South American subduction zone.

and may not be the sole set of events leading to changes in relative plate motion (**Figure 8**) in all ocean basins.

CONCLUSIONS

Our combined plate tectonic, plate boundary topology, and oceanic paleo-age grid model builds upon and extends the model by Seton et al. (2012) in several ways. Global RMS absolute plate velocities are generally lower because of improvements in both relative and absolute plate motion models. The model is extended from 200 to 230 Ma into the Triassic, better capturing a period of supercontinent stability, from 230 to 200 Ma, when the breakup of Pangea commenced. The model assimilates numerous major regional plate model improvements published since 2012, both in major ocean basins as well as in complex regions such as the Caribbean, the Scotia Sea, the western and central Tethys, and Southeast Asia including the eastern Tethys. Refined oceanic paleo-age grids allow an improved analysis of the effects of the lateral age profiles of subducting plates on trench rollback and plate driving forces. Relatively high mean absolute plate motion rates around 9–10 cm yr^{-1} between 140 and 120 Ma may be related to transient plate motion accelerations driven by the successive emplacement of a sequence of LIPs during that time, weakening lithosphere-asthenosphere coupling and thus lubricating the bottom boundary of the plates on which the plume heads impinged. A global event around 100 Ma may mainly reflect the initiation of Andean-style subduction along continental Eurasia, with ongoing and contemporaneous intraoceanic subduction in the Neo-Tethys (Gibbons et al. 2015). Our model supports a regional plate motion event around 70 Ma, centered on Africa, and a plate tectonic event around 50 Ma that expresses itself not only in regional relative plate motion changes in most ocean basins (see also the summary in Whittaker et al. 2007) but also in a decrease in global absolute RMS plate speeds around that time. The origin of that event remains to be explored, as it does not appear to directly reflect the Hawaiian–Emperor Bend, which mainly records the slowdown of southward motion of the Hawaii plume (Tarduno 2007, Wright et al. 2015). However, the Hawaiian–Emperor Bend could still include a component of absolute plate motion change, as the reorganization of the mantle flow processes beneath the Pacific that led to the slowdown of the Hawaiian plume may have had a feedback effect on plate-mantle coupling and absolute plate motions. The only two truly global tectonic events our analysis reveals are the major RMS speed increase from 140 to 120 Ma and the decrease in RMS speed observed at around 50 Ma. Both of these events may reflect major changes in plate-mantle coupling.

Our global plate model analysis highlights that the 50-year-old theory of plate tectonics still falls short in explaining how interactions between the convecting mantle and the plates cause major perturbations in plate driving forces and global tectonic events. A major challenge for the future is improved global modeling and an enhanced understanding of plate driving forces. This will eventually need to include the coupling of the plates both to the deep mantle and to the shallow asthenosphere, including effects ranging from pressure-driven Poiseuille flow at shorter wavelengths to dominantly shear-driven Couette flow at longer wavelengths (Colli et al. 2014, Hoink et al. 2011) in a global spherical model that considers all plates, the history of subduction, and regional differences in lithospheric and asthenospheric thickness.

Our model provides initial or time-dependent surface boundary conditions for mantle convection models, and for providing tectonic boundary conditions through time for models of basin and passive margin evolution. The model will also be a useful basis for future spatiotemporal data analysis, facilitating an analysis of associations between plate tectonic settings and igneous geochemistry data from the EarthChem Portal (**http://www.earthchem.org**) (Lehnert et al. 2000), or paleoenvironmental indicators based on fossils and paleobiology data (**http://fossilworks.org** and

http://paleobiodb.org), using emerging machine learning methods (Peters et al. 2014). Lastly, this model will also be valuable as an educational resource; jointly with the GPlates community plate reconstruction software (Boyden et al. 2011), it is useful for learning in an interactive and intuitive way how plate tectonics works, as the model can be played back, interrogated, manipulated, and changed, focusing either on the entire globe or on regional areas of interest.

All components of our model, including model animations, are made available as open-access files to the community, including the static polygons that define the present-day outlines of all plates involved in the model, the global rotation file, the continuously closing time-dependent plate boundaries, and the oceanic paleo-age grids in 1 Myr intervals from 230 Ma to the present (see Supplemental Material; follow the Supplemental Material link in the online version of this article or at **http://www.annualreviews.org/**).

Supplemental Material

DISCLOSURE STATEMENT

The authors are not aware of any affiliations, memberships, funding, or financial holdings that might be perceived as affecting the objectivity of this review.

ACKNOWLEDGMENTS

R.D.M. and S.E.W. were supported by Australian Research Council (ARC) grants DP130101946 and IH130200012, S.Z. by ARC grant IH130200012, M.S. by ARC grant FT130101564, K.J.M. and K.T.M. by ARC grant DP130101946, S.E.W., J.C., and M.H. by ARC grant FL0992245, and N.M.W. and N.B.M. by Australian Postgraduate Awards. We thank Michael G. Tetley for providing technical support and workflow enhancement that improved the management of seafloor isochrons and other GPlates-related geometries. GPlates (**http://www.gplates.org**) can be downloaded on an open-source and cross-platform (Windows, Mac, and Linux) basis. G.E.S. acknowledges support from the Research Council of Norway through its Centres of Excellence funding scheme, project 22372. D.J.B.'s current affiliation is the Institut für Geophysik, ETH Zürich, 8092 Zürich, Switzerland. We thank the reviewers for their constructive comments, which helped improve the paper considerably.

LITERATURE CITED

Amante C, Eakins BW. 2009. *ETOPO1 1 arc-minute global relief model: procedures, data sources and analysis*. NOAA Tech. Memo. NESDIS NGDC-24, Mar. Geol. Geophys. Div., Natl. Geophys. Data Cent., Natl. Ocean. Atmos. Admin. (NOAA), Boulder, CO

Arculus RJ, Ishizuka O, Bogus KA, Gurnis M, Hickey-Vargas R, et al. 2015. A record of spontaneous subduction initiation in the Izu-Bonin-Mariana arc. *Nat. Geosci.* 8:728–33

Barnett-Moore N, Müller RD, Williams SE, Skogseid J, Seton M. 2016. A reconstruction of the North Atlantic since the earliest Jurassic. *Basin Res.* In review

Bird P. 2003. An updated digital model of plate boundaries. *Geochem. Geophys. Geosyst.* 4:1027

Boschman LM, van Hinsbergen DJ, Torsvik TH, Spakman W, Pindell JL. 2014. Kinematic reconstruction of the Caribbean region since the Early Jurassic. *Earth-Sci. Rev.* 138:102–36

Bower DJ, Gurnis M, Seton M. 2013. Lower mantle structure from paleogeographically constrained dynamic Earth models. *Geochem. Geophys. Geosyst.* 14:44–63

Boyden JA, Müller RD, Gurnis M, Torsvik TH, Clark JA, et al. 2011. Next-generation plate-tectonic reconstructions using GPlates. In *Geoinformatics: Cyberinfrastructure for the Solid Earth Sciences*, ed. GR Keller, C Baru, pp. 95–114. Cambridge, UK: Cambridge Univ. Press

Butterworth NP, Müller RD, Quevedo L, O'Connor JM, Hoernle K, Morra G. 2014a. Pacific Plate slab pull and intraplate deformation in the early Cenozoic. *Solid Earth* 5:757–77

Butterworth NP, Talsma AS, Müller RD, Seton M, Bunge HP, et al. 2014b. Geological, tomographic, kinematic and geodynamic constraints on the dynamics of sinking slabs. *J. Geodyn.* 73:1–13
Cande SC, Kent DV. 1995. Revised calibration of the geomagnetic polarity timescale for the Late Cretaceous and Cenozoic. *J. Geophys. Res.* 100(B4):6093–95
Cande SC, Patriat P. 2015. The anticorrelated velocities of Africa and India in the Late Cretaceous and early Cenozoic. *Geophys. J. Int.* 200:227–43
Cannon J, Lau E, Müller R. 2014. Plate tectonic raster reconstruction in GPlates. *Solid Earth* 5:741–55
Capitanio F, Faccenna C, Funiciello R. 2009. The opening of Sirte basin: result of slab avalanching? *Earth Planet. Sci. Lett.* 285:210–16
Channell JET. 1995. Recalibration of the geomagnetic polarity timescale. *Rev. Geophys.* 33:161–68
Christeson G, Van Avendonk H, Norton I, Snedden J, Eddy D, et al. 2014. Deep crustal structure in the eastern Gulf of Mexico. *J. Geophys. Res. Solid Earth* 119:6782–801
Cogne JP, Humler E, Courtillot V. 2006. Mean age of oceanic lithosphere drives eustatic sea-level change since Pangea breakup. *Earth Planet. Sci. Lett.* 245:115–22
Colli L, Stotz I, Bunge HP, Smethurst M, Clark S, et al. 2014. Rapid South Atlantic spreading changes and coeval vertical motion in surrounding continents: evidence for temporal changes of pressure-driven upper mantle flow. *Tectonics* 33:1304–21
Coltice N, Rolf T, Tackley P, Labrosse S. 2012. Dynamic causes of the relation between area and age of the ocean floor. *Science* 336:335–38
Coltice N, Seton M, Rolf T, Müller R, Tackley PJ. 2013. Convergence of tectonic reconstructions and mantle convection models for significant fluctuations in seafloor spreading. *Earth Planet. Sci. Lett.* 383:92–100
Cox A, Hart BR. 1986. *Plate Tectonics: How It Works*. Palo Alto, CA: Blackwell
Dodd SC, Mac Niocaill C, Muxworthy AR. 2015. Long duration (>4 Ma) and steady-state volcanic activity in the early Cretaceous Paraná-Etendeka Large Igneous Province: new palaeomagnetic data from Namibia. *Earth Planet. Sci. Lett.* 414:16–29
Doubrovine PV, Steinberger B, Torsvik TH. 2012. Absolute plate motions in a reference frame defined by moving hot spots in the Pacific, Atlantic, and Indian oceans. *J. Geophys. Res.* 117:B09101
Eagles G, Jokat W. 2014. Tectonic reconstructions for paleobathymetry in Drake Passage. *Tectonophysics* 611:28–50
Fournier M, Chamot-Rooke N, Petit C, Huchon P, Al-Kathiri A, et al. 2010. Arabia-Somalia plate kinematics, evolution of the Aden-Owen-Carlsberg triple junction, and opening of the Gulf of Aden. *J. Geophys. Res.* 115:B04102
Gee J, Kent D. 2007. Source of oceanic magnetic anomalies and the geomagnetic polarity timescale. In *Treatise on Geophysics*, Vol. 5: *Geomagnetism*, ed. M Kono, pp. 455–507. Amsterdam: Elsevier. 1st ed.
Gibbons A, Zahirovic S, Müller R, Whittaker J, Yatheesh V. 2015. A tectonic model reconciling evidence for the collisions between India, Eurasia and intra-oceanic arcs of the central-eastern Tethys. *Gondwana Res.* 28:451–92
Gibbons AD, Whittaker JM, Müller RD. 2013. The breakup of East Gondwana: assimilating constraints from Cretaceous ocean basins around India into a best-fit tectonic model. *J. Geophys. Res. Solid Earth* 118:808–22
Goes S, Capitanio FA, Morra G. 2008. Evidence of lower mantle slab penetration phases in plate motions. *Nature* 451:981–84
Granot R, Cande S, Stock J, Damaske D. 2013. Revised Eocene-Oligocene kinematics for the West Antarctic rift system. *Geophys. Res. Lett.* 40:279–84
Granot R, Dyment J. 2015. The Cretaceous opening of the South Atlantic Ocean. *Earth Planet. Sci. Lett.* 414:156–63
Granot R, Dyment J, Gallet Y. 2012. Geomagnetic field variability during the Cretaceous Normal Superchron. *Nat. Geosci.* 5:220–23
Gurnis M, Turner M, Zahirovic S, DiCaprio L, Spasojevic S, et al. 2012. Plate tectonic reconstructions with continuously closing plates. *Comput. Geosci.* 38:35–42
Heine C, Zoethout J, Müller RD. 2013. Kinematics of the South Atlantic rift. *Solid Earth* 4:215–53
Hellinger S. 1981. The uncertainties of finite rotations in plate tectonics. *J. Geophys. Res. Solid Earth* 86:9312–18

Hoink T, Jellinek A, Lenardic A. 2011. Viscous coupling at the lithosphere-asthenosphere boundary. *Geochem. Geophys. Geosyst.* 12:Q0AK02
Hosseinpour M, Müller RD, Williams SE, Whittaker JM. 2013. Full-fit reconstruction of the Labrador Sea and Baffin Bay. *Solid Earth* 4:461–79
Hosseinpour M, Williams SE, Seton M, Barnett-Moore N, Müller RD. 2016. Tectonic evolution of Western Tethys from Jurassic to present day: coupling geological and geophysical data with seismic tomography models. *Int. Geol. Rev.* In press
Huber M, Goldner A. 2012. Eocene monsoons. *J. Asian Earth Sci.* 44:3–23
Iaffaldano G, Hawkins R, Bodin T, Sambridge M. 2014a. REDBACK: open-source software for efficient noise-reduction in plate kinematic reconstructions. *Geochem. Geophys. Geosyst.* 15:1663–70
Iaffaldano G, Hawkins R, Sambridge M. 2014b. Bayesian noise-reduction in Arabia/Somalia and Nubia/Arabia finite rotations since ~20 Ma: implications for Nubia/Somalia relative motion. *Geochem. Geophys. Geosyst.* 15:845–54
Kirkwood BH, Royer JY, Chang TC, Gordon RG. 1999. Statistical tools for estimating and combining finite rotations and their uncertainties. *Geophys. J. Int.* 137:408–28
Kneller EA, Johnson CA, Karner GD, Einhorn J, Queffelec TA. 2012. Inverse methods for modeling non-rigid plate kinematics: application to Mesozoic plate reconstructions of the Central Atlantic. *Comput. Geosci.* 49:217–30
Kumar P, Yuan X, Kumar MR, Kind R, Li X, Chadha R. 2007. The rapid drift of the Indian tectonic plate. *Nature* 449:894–97
Larson RL, Chase CG. 1972. Late Mesozoic evolution of the western Pacific Ocean. *Geol. Soc. Am. Bull.* 83:3627–44
Lehnert K, Su Y, Langmuir C, Sarbas B, Nohl U. 2000. A global geochemical database structure for rocks. *Geochem. Geophys. Geosyst.* 1:1012
Lowrie W, Kent DV. 2004. Geomagnetic polarity timescales and reversal frequency regimes. *Geophys. Monogr. Ser.* 145:117–29
Maher SM, Wessel P, Müller RD, Williams SE, Harada Y. 2015. Absolute plate motion of Africa around Hawaii-Emperor bend time. *Geophys. J. Int.* 201:1743–64
Matthews KJ, Maloney KT, Zahirovic S, Williams SE, Seton M, Müller RD. 2016a. Global plate boundary evolution and kinematics since the late Paleozoic. *Glob. Planet. Change.* Submitted
Matthews KJ, Müller RD, Sandwell DT. 2016b. Oceanic microplate formation records the onset of India–Eurasia collision. *Earth Planet. Sci. Lett.* 433:204–14
Matthews KJ, Müller RD, Wessel P, Whittaker JM. 2011. The tectonic fabric of the ocean basins. *J. Geophys. Res.* 116:B12109
Matthews KJ, Seton M, Müller RD. 2012. A global-scale plate reorganization event at 105–100 Ma. *Earth Planet. Sci. Lett.* 355:283–98
Matthews KJ, Williams SE, Whittaker JM, Müller RD, Seton M, Clarke GL. 2015. Geologic and kinematic constraints on Late Cretaceous to mid Eocene plate boundaries in the southwest Pacific. *Earth-Sci. Rev.* 140:72–107
Morra G, Seton M, Quevedo L, Müller RD. 2013. Organization of the tectonic plates in the last 200 Myr. *Earth Planet. Sci. Lett.* 373:93–101
Müller RD, Dutkiewicz A, Seton M, Gaina C. 2013. Seawater chemistry driven by supercontinent assembly, breakup, and dispersal. *Geology* 41:907–10
Müller RD, Dutkiewicz A, Seton M, Gaina C. 2014. Seawater chemistry driven by supercontinent assembly, breakup and dispersal: reply. *Geology* 42:e335
Müller RD, Roest WR, Royer JY, Gahagan LM, Sclater JG. 1997. Digital isochrons of the world's ocean floor. *J. Geophys. Res.* 102(B2):3211–14
Müller RD, Roest WR, Royer JY. 1998. Asymmetric sea-floor spreading caused by ridge-plume interactions. *Nature* 396:455–59
Müller RD, Sdrolias M, Gaina C, Steinberger B, Heine C. 2008. Long-term sea-level fluctuations driven by ocean basin dynamics. *Science* 319:1357–62
Nakanishi M, Tamaki K, Kobayashi K. 1992. A new Mesozoic isochron chart of the northwestern Pacific Ocean: paleomagnetic and tectonic implications. *Geophys. Res. Lett.* 19:693–96

O'Neill C, Müller D, Steinberger B. 2005. On the uncertainties in hot spot reconstructions and the significance of moving hot spot reference frames. *Geochem. Geophys. Geosyst.* 6:Q04003
Peters SE, Zhang C, Livny M, Ré C. 2014. A machine reading system for assembling synthetic paleontological databases. *PLOS ONE* 9:e113523
Prokoph A, El Bilali H, Ernst R. 2013. Periodicities in the emplacement of large igneous provinces through the Phanerozoic: relations to ocean chemistry and marine biodiversity evolution. *Geosci. Front.* 4:263–76
Qin X, Müller RD, Cannon J, Landgrebe TCW, Heine C, et al. 2012. The GPlates Geological Information Model and Markup Language. *Geosci. Instrum. Methods Data Syst.* 2:365–428
Quirk DG, Hertle M, Jeppesen JW, Raven M, Mohriak WU, et al. 2013. Rifting, subsidence and continental break-up above a mantle plume in the central South Atlantic. *Geol. Soc. Lond. Spec. Publ.* 369:185–214
Rona PA, Richardson ES. 1978. Early Cenozoic global plate reorganization. *Earth Planet. Sci. Lett.* 40:1–11
Sandwell DT, Müller RD, Smith WH, Garcia E, Francis R. 2014. New global marine gravity model from CryoSat-2 and Jason-1 reveals buried tectonic structure. *Science* 346:65–67
Schellart W, Stegman D, Freeman J. 2008. Global trench migration velocities and slab migration induced upper mantle volume fluxes: constraints to find an Earth reference frame based on minimizing viscous dissipation. *Earth-Sci. Rev.* 88:118–44
Schettino A, Turco E. 2011. Tectonic history of the western Tethys since the Late Triassic. *Geol. Soc. Am. Bull.* 123:89–105
Seton M, Flament N, Whittaker J, Müller RD, Gurnis M, Bower DJ. 2015. Ridge subduction sparked reorganization of the Pacific plate-mantle system 60–50 million years ago. *Geophys. Res. Lett.* 42:1732–40
Seton M, Mortimer N, Williams SE, Quilty P, Gans P, et al. 2016. Melanesian back-arc basin and arc development: implication for Ontong Java Plateau timing. *Gondwana Res.* In review
Seton M, Müller RD, Zahirovic S, Gaina C, Torsvik TH, et al. 2012. Global continental and ocean basin reconstructions since 200 Ma. *Earth-Sci. Rev.* 113:212–70
Seton M, Whittaker JM, Wessel P, Müller RD, DeMets C, et al. 2014. Community infrastructure and repository for marine magnetic identifications. *Geochem. Geophys. Geosyst.* 15:1629–41
Shephard GE, Bunge HP, Schuberth BS, Müller R, Talsma A, et al. 2012. Testing absolute plate reference frames and the implications for the generation of geodynamic mantle heterogeneity structure. *Earth Planet. Sci. Lett.* 317:204–17
Shephard GE, Flament N, Williams SE, Seton M, Gurnis M, Müller RD. 2014. Circum-Arctic mantle structure and long-wavelength topography since the Jurassic. *J. Geophys. Res. Solid Earth* 119:7889–908
Shephard GE, Müller RD, Seton M. 2013. The tectonic evolution of the Arctic since Pangea breakup: integrating constraints from surface geology and geophysics with mantle structure. *Earth-Sci. Rev.* 124:148–83
Steinberger B, O'Connell RJ. 1998. Advection of plumes in mantle flow: implications for hot spot motion, mantle viscosity and plume distributions. *Geophys. J. Int.* 132:412–34
Steinberger B, Torsvik TH. 2008. Absolute plate motions and true polar wander in the absence of hotspot tracks. *Nature* 452:620–23
Tarduno JA. 2007. On the motion of Hawaii and other mantle plumes. *Chem. Geol.* 241:234–47
Torsvik TH, Müller RD, Van der Voo R, Steinberger B, Gaina C. 2008. Global plate motion frames: toward a unified model. *Rev. Geophys.* 46:RG3004
Torsvik TH, Steinberger B, Gurnis M, Gaina C. 2010. Plate tectonics and net lithosphere rotation over the past 150 My. *Earth Planet. Sci. Lett.* 291:106–12
Torsvik TH, Van der Voo R, Preeden U, Mac Niocaill C, Steinberger B, et al. 2012. Phanerozoic polar wander, palaeogeography and dynamics. *Earth-Sci. Rev.* 114:325–68
van der Meer DG, Spakman W, van Hinsbergen DJ, Amaru ML, Torsvik TH. 2010. Towards absolute plate motions constrained by lower-mantle slab remnants. *Nat. Geosci.* 3:36–40
Van der Voo R, van Hinsbergen DJ, Domeier M, Spakman W, Torsvik TH. 2015. Latest Jurassic–earliest Cretaceous closure of the Mongol-Okhotsk Ocean: a paleomagnetic and seismological-tomographic analysis. *Geol. Soc. Am. Spec. Pap.* 513:SPE513–19
Wessel P, Kroenke L. 2008. Pacific absolute plate motion since 145 Ma: an assessment of the fixed hot spot hypothesis. *J. Geophys. Res.* 113:B06101
Wessel P, Matthews KJ, Müller RD, Mazzoni A, Whittaker JM, et al. 2015. Semiautomatic fracture zone tracking. *Geochem. Geophys. Geosyst.* 16:2462–72

Whittaker JM, Afonso JC, Masterton S, Müller RD, Wessel P, et al. 2015. Long-term interaction between mid-ocean ridges and mantle plumes. *Nat. Geosci.* 8:479–83

Whittaker JM, Müller RD, Leitchenkov G, Stagg H, Sdrolias M, et al. 2007. Major Australian-Antarctic plate reorganization at Hawaiian-Emperor bend time. *Science* 318:83–86

Whittaker JM, Williams SE, Müller RD. 2013. Revised tectonic evolution of the Eastern Indian Ocean. *Geochem. Geophys. Geosyst.* 14:1891–909

Williams SE, Flament N, Müller RD, Butterworth N. 2015. Absolute plate motions since 130 Ma constrained by subduction zone kinematics. *Earth Planet. Sci. Lett.* 418:66–77

Williams SE, Whittaker JM, Müller RD. 2011. Full-fit, palinspastic reconstruction of the conjugate Australian-Antarctic margins. *Tectonics* 30:TC6012

Wright NM, Müller RD, Seton M, Williams SE. 2015. Revision of Paleogene plate motions in the Pacific and implications for the Hawaiian-Emperor bend. *Geology* 43:455–58

Wright NM, Seton M, Williams SE, Müller RD. 2016. The Late Cretaceous to recent tectonic history of the Pacific Ocean basin. *Earth-Sci. Rev.* 154:138–73

Zahirovic S, Müller RD, Seton M, Flament N. 2015. Tectonic speed limits from plate kinematic reconstructions. *Earth Planet. Sci. Lett.* 418:40–52

Zahirovic S, Seton M, Müller RD. 2014. The Cretaceous and Cenozoic tectonic evolution of Southeast Asia. *Solid Earth* 5:227–73